T.C.

ALTINBAŞ UNIVERSITY

Electrical and Computer Engineering

MINIATURE MICROSTRIP ANTENNA FOR WIRELESS COMMUNICATION USING FRACTAL AND NON-FRACTAL GEOMETRIES

Ali Rashid AbdulHameed

Master Thesis

Supervisor:
Prof. Dr. Osman Nuri Ucan

Istanbul, 2019

MINIATURE MICROSTRIP ANTENNA FOR WIRELESS COMMUNICATION USING FRACTAL AND NON-FRACTAL GEOMETRIES

by

Ali Rashid AbdulHameed

Electrical and Computer Engineering

Submitted to the Graduate School of Science and Engineering

in partial fulfillment of the requirements for the degree of

Master of Science

ALTINBAŞ UNIVERSITY

[2019]

This is to certify that we have read this thesis and that in our opinion it is fully adequate, in scope and quality, as a thesis for the degree of Master of Science.

Dr. Yaqeen Sabah MEZAAL	Prof. Dr. Osman Nuri UCAN

Examining Committee Members (first name belongs to the chairperson of the jury and the second name belongs to supervisor)

Prof. Dr. Osman Nuri UCAN	School of Engineering and Natural Sciences, Altinbas University	_____
Asst. Prof. Dr. Muhammad ILYAS	School of Engineering and Natural Sciences, Altinbas University	_____
Prof. Dr. Hasan H. BALIK	Air Force Academy, National Defense University	_____

I certify that this thesis satisfies all the requirements as a thesis for the degree of.....

Asst. Prof. Cagatay AYDIN

Head of Department

Prof. Dr. Oguz BAYAT

Director

Approval Date of Graduate School of Science and Engineering: ____/____/____

I hereby declare that all information in this document has been obtained and presented in accordance with academic rules and ethical conduct. I also declare that, as required by these rules and conduct, I have fully cited and referenced all material and results that are not original to this work.

Ali Rashid AbdulHameed

DEDICATION

First of all, praise is to Allah for everything without his great assistance the work wouldn`t have been finished.

I dedicate this work to my father and mother foe their supporting, help and to my sister Zahraa

MY FAMILY YOU MY STRENGTH.

ACKNOWLEDGEMENTS

I would like to express my thanks and my great respect and appreciation to my supervisor Prof. Dr. Osman Nuri Ucan and my co-supervisor Dr.Yaqeen Sabah Mezaal for their great guidance and support to get on best results for this work.

I would like to thank Ms. Seevan Fahmi Abdulkareem for her assistance and support me in my research.

ABSTRACT

MINIATURE MICROSTRIP ANTENNA FOR WIRELESS COMMUNICATION USING FRACTAL AND NON-FRACTAL GEOMETRIES

Alsalihi, Ali Rashid

M.S., Electrical and Computer Engineering, Altınbaş University,

Supervisor: Prof. Dr. Osman Nuri Ucan

Co-Supervisor: Dr. Yaqeen Sabah Mezaal

Date: 06/2019

Pages: 47

In this thesis, two microstrip antennas based on quasi fractal geometries are presented by using FR4 substrate material. They have clearly multi band response for modern wireless applications. This antenna has modeled using AWR simulator based on quasi-fractal topology. The shaped antenna has compacted size and acceptable electrical specifications that are suitable for numerous fixed and handheld wireless systems.

The third designed device is printed slot antenna and does not stand for microstrip antenna just the feed is microstrip since the designed stair-step topology has been printed in the ground plane of FR4 substrate. Based on the parametric study of third antenna, its response has only single and dual potential bands. Here in this study, single band response at strategic frequency of 5.75 GHz has been adopted with fabrication and measurements.

Keywords: Microstrip Antenna,AWR Simulator, CST Simulator, FR4.

TABLE OF CONTENTS

Pages

LIST OF TABLES

Pages

LIST OF FIGURES

Pages

LIST OF ABBREVIATIONS

AWR	:	Applied Wave Research
BW	:	Bandwidth
CPW	:	Co-Planar Waveguide
CST	:	Computer Simulation Technique
RF	:	Radio Frequency
RL	:	Return Loss
MSA	:	Microstrip Antenna
PCB	:	Printed-Circuit Board
GSM	:	Global System for Mobile Communication

1. INTRODUCTION AND LITERATURE SURVEY

1.1 INTRODUCTION

Recently, an increasing number of communication services become available below (6) GHz frequency range. On the other hand, more wireless systems are now multifunctional. Usually, antennas operate at single frequency band, in which a different antenna will be required for different applications. This is going to lead to a problem due to the limited space; especially most of the manufacturers tend to produce compact and miniaturized systems. For the purpose of overcoming this issue, multiband antennas could be utilized in the case when single antenna operates at several frequency bands [1].

Utilizing fractal shapes in antenna geometries could be considered as one method for constructing multi-band antennas. These modern antennas require a function of offering a multi or dual band operations, in addition to simple integration with the circuit of the system, compact size and uncomplicated structure, as shown in Figure 1.1. In Figure 1.1, Sierpinski carpet fractal geometry has been used to form the shape of a multi-band microstrip antenna of a mobile system. The antenna covers the GSM frequency bands of 900, 1800, and 1900 MHz GSM [2].

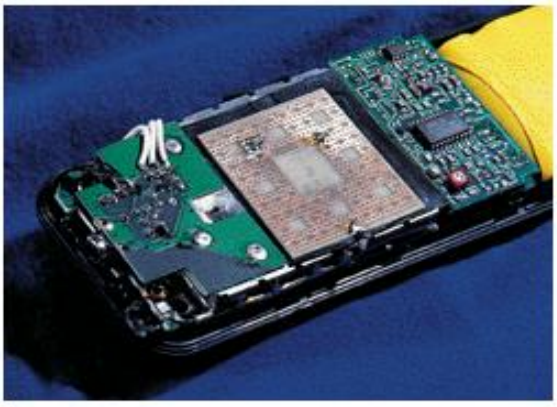

Figure 1.1: A photo of the Sierpinski carpet used to fabricate an internal antenna of a mobile phone covering the 900 MHz, 1800 MHz, and 1900 MHz bands [2].

Microstrip antennas have been found to be attractive to antenna designers because of they are cost-effective, low-profile and lightweight. On the other hand, narrow bandwidth is considered as a

main drawback of microstrip. To overcome this drawback, slot structure with various shapes were applied to design broadband / wideband printed antennas. Therefore, it seems logical to employ a hybrid of these techniques; slot structures and fractal geometries for designing multi-band antenna with enhanced resonant bandwidth.

Fractal geometry is utilized in designing antennas for the purpose of producing multi-band and compact antennas benefit from their exceptional features; space filling and self-similarity, as shown in Figure 1.2.

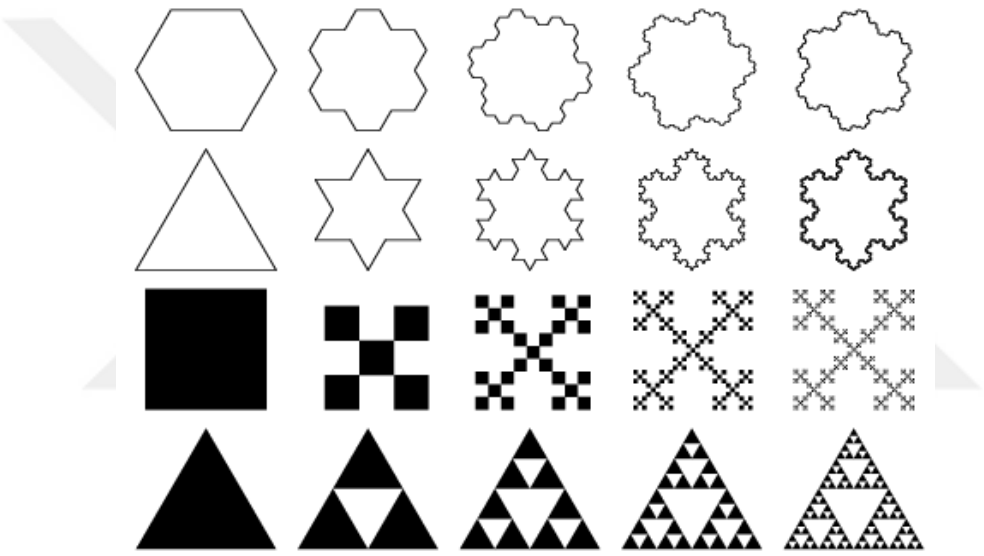

Figure 1.2: Some of representative types of the most commonly used fractal geometries together with the corresponding steps of growth up to the fourth iteration levels [3].

1.2 FRACTAL-BASED SLOT ANTENNAS

Common fractal geometry methods including Minkowski, Koch, Hilbert, Sierpinski, Cantor as well as other fractal curves were effectively utilized for producing multi and dual band printed slot antennas for different wireless applications.

In that regard, applications related to fractal geometry in designing slot printed antenna could be categorized into 2 types. In the first one, direct fractal geometry application was used. In such

situation, all antenna slot structures are made by fractal geometries. The multi-band performance related to these antennas was extracted almost directly with no necessity for slot shape modification or tuning elements. In the second one, slot structures are considered as a combination related to Euclidian structures, including rectangle, square, triangle and additional polygons, in addition to fractal geometry that is superimposed on such structures, in which all line segments will be replaced via fractal curve with specific level of iteration. Fractals produced by several Euclidean geometries including triangle, circle and others, were used for producing dual-band antennas for many applications related to communication field.

2. MICROSTRIP ANTENNAS AND FEEDING TECHNIQUES

2.1 INTRODUCTION

This chapter presents a study related to microstrip antennas. This involves the weaknesses and capabilities related to such antennas in different wireless applications. The main parameters managing the performance of the antenna were examined along with design equations regarding the microstrip patch antenna. The frequently used antenna feed approaches were assessed. A summarization is provided regarding an evaluation of the antenna feed approaches.

2.2 MICROSTRIP ANTENNAS

In 1952, the MSA concept was suggested by Deschamps. Nevertheless, in the 70s, Howell and Munson developed practical antennas [4].

The many features of MSA, like simplicity of fabrication through the use of printed-circuit technologies, small volume, lightweight, resulted in designing numerous configurations for many implementations. With rising necessities for mobile and personal communications, the need for low profile and smaller antenna brought microstrip antennas to the front.

The radiation from MSA might happen from fringing fields between ground plane and patch periphery. Length L regarding the rectangular patch for fundamental mode excitation of TM10 is little less than $\lambda/2$, with the wave-length in dielectric medium is λ, that in relation to the free space wave-length λ_o is specified as $\lambda_o / \sqrt{\varepsilon_e}$, here ε_e can be defined as the effective dielectric constant related to micro-strip line of the width W.

ε_e is little smaller compared to the substrate's dielectric constant ε_r since the fringing fields from patch to ground plane aren't confined in only the dielectric however they are spread in air as well. For the purpose of enhancing fringing fields from patch, that cause radiation, patch's width W will be increased. The increase of substrate thickness h and the reduction of ε_r will enhance the fringing fields. Substrates with thicker h and lower ε_r and microstrip patches with larger width are used by MSA [4].

MSA are essentially narrowband. The standard MSA bandwidth is about 4-7 percent. A significant number of studies were carried out for the purpose of developing MSA.

For increasing the impedance bandwidth, the methods employed are basically variations of 3 methods [5]:

- Increasing the volume of antenna via geometry alterations which focus of increasing the volume under patch (to increase thickness *h*), add more coupled resonators, decrease substrate dielectric constant.
- Application of matching network.
- Perturbing the geometry of antenna geometry for relocating or creating resonances through the use of slots and shorts in antenna.

A lot of applications use MSAs because of their advantages. The communication and telemetry antennas on missiles must be conformal and thin and are they are usually MSAs. Small arrays of microstrip radiators are used by radar altimeters. Additional aircraft-associated applications such as satellite communication and antennas for telephone. The systems of satellite imaging use microstrip arrays. The patch antennas were applied on links of communication between satellites and ships or buoys. Because of their thing profile, MSAs are used by the systems of smart weapons systems. GPS, GSM and pagers are the main users of MSA [4].

2.2.1 Microstrip Patch Antenna

In its simplest form, micro-strip patch antennas, have radiating patch on a side of dielectric substrate that has a ground plane on the other side as displayed in the Figure 2.1.

Mostly, a patch is composed of a conducting material like gold or copper and might take various shapes. Feed line and the radiating patch are typically etched or printed on dielectric substrate [6].

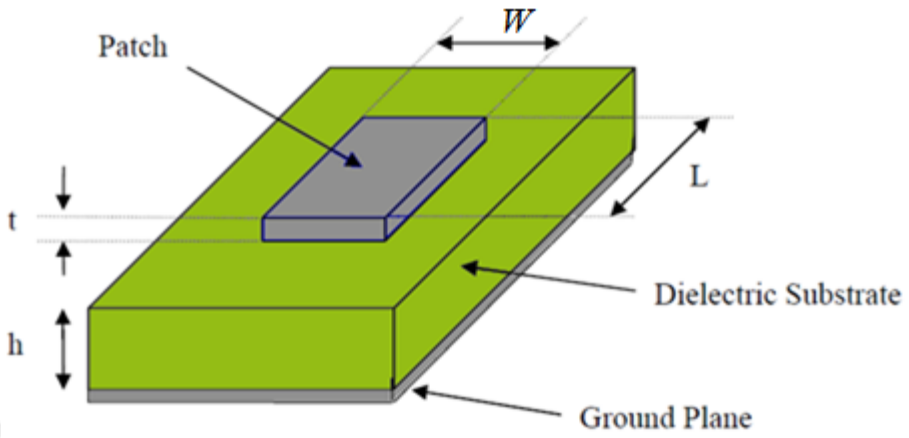

Figure 2.1: The basis structure of a microstrip patch antenna [6].

For rectangular patch, the patch's width W is usually $0.3333\lambda_o < W < 0.5\ \lambda_o$, here λ_o can be defined as the free-space wave length. The patch is selected extremely thin in a manner that $t << \lambda_o$ (t can be defined as the thickness of the patch). The dielectric substrate's height h is typically $0.003\ \lambda_o \leq h \leq 0.05\ \lambda_o$. The substrate's dielectric constant (ε_r) is usually in the range $2.2 \leq \varepsilon_r \leq 16$.

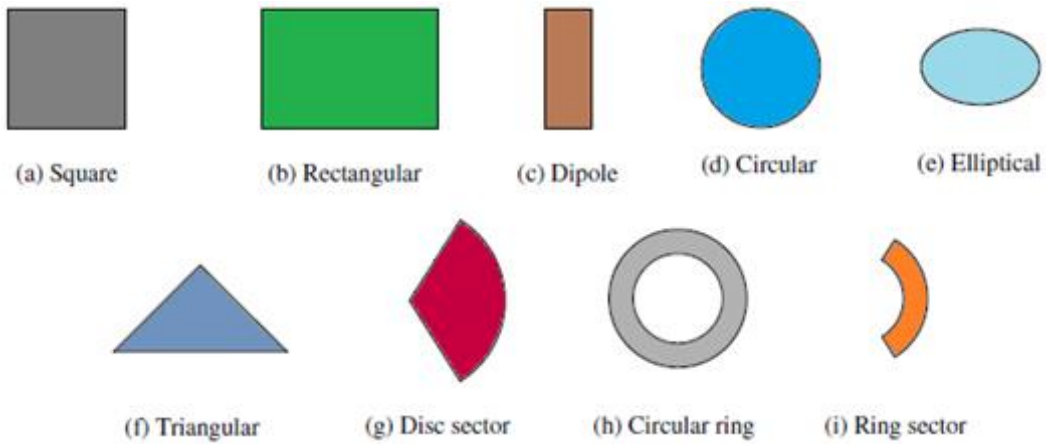

Figure 2.2: Common shapes of microstrip patch elements [6].

Micro-strip patch antenna radiates mainly due to the fringing fields between ground plane and patch edge. For optimum performance of antennas, it is desired having thick dielectric substrate

with low dielectric constant due to the fact that this offers better effectiveness, optimum radiation and more bandwidth. Nevertheless, larger size antennas will be the result of these configurations.

For the purpose of designing compact Micro-strip patch antennas, higher dielectric constants should be deployed that are less effective and lead to smaller bandwidth. Therefore, cooperation should be achieved between the performance and dimensions of antennas [4].

2.2.2 Features and Limitations of Microstrip Antennas Features

MSAs and arrays were the main focus for many engineers and studies and were utilized broadly in microwave systems and RF, like biomedical systems, navigations, communication, remote sensing and radars. There are various forms for MSAs, including slot, dipole, patch, or traveling-wave structure, developed for particular applications [4], [7].

Patch-like or patch radiators feature special properties and were examined deeply. They provide some significant features:

- *Low profile*. The thickness that is related to the microstrip patch antennas is typically less than 0.03 λ_o (λ_o can be defined as the operating wave length in free-space).
- *Adaptability regarding the surface of substrate*. Micro-strip patch antenna could be of non-planer or planar surfaces, which might totally comply with the surface of dielectric substrate to which it is attached.
- *Lightweight*. Micro-strip patch antennas are typically composed of perfectly electrically conducting (PEC) foil which is affixed on dielectric substrate.
- *Integration with other circuits*. It is simple to totally integrate micro-strip patch antennas on printed-circuit board (PCB) with other planar circuits.
- *Low costs*. Micro-strip patch antennas are usually fabricated through the use of low-cost printed circuit approach. Substrate is typically the most expensive part of the antennas.
- *Versatility*. Micro-strip patch antennas are versatile with regard to operating mode, resonant frequency, polarization, impedance and radiation pattern, through choice of shape and feeding method.

A lot of methods, including adding shorting pins, slotting and loading patch, varactor diodes, or presenting parasitic elements, could be utilized to antennas.

- They enable triple- and dual -frequency operations.

- They enable circular and linear polarization.
- They could be compact to be used in personal mobile communication.

Limitations of microstrip patch antenna

There are some drawbacks in Microstrip patch antennas in comparison to standard antennas. Several of their main drawbacks are specified below [8]:

- It is complicated to achieve polarization purity
- Narrow bandwidth.
- Low effectiveness.
- Surface wave excitation
- Extraneous radiation from junctions and feeds.
- Inadequate end fire radiator apart from tapered slot antenna.
- Low Gain.
- The majority of MSAs radiate into half-space.
- Complex feed structures are needed for high-efficiency arrays.
- Weak capacity for power handling.

Losses related to antennas are represented by the quality factor (Q factor), low effectiveness and narrow bandwidth are caused by large Q factor. The Q factor of Microstrip patch antennas is extremely high. The increase in the thickness related to dielectric substrate will decrease the Q factor. Yet, when increasing the thickness, an increasing part regarding the overall power which is delivered via the source goes into the surface wave. The contribution of the surface wave could be counted as undesirable loss of power because it is eventually scattered at dielectric bends and result in regression of the antenna features. Nevertheless, using photonic bandgap structures will minimize these surface waves. Additional issues including low power handling capability and low gain could be addressed through the use of array configuration for elements.

2.2.3 Substrates

Substrates have a variety of available dielectric materials. Significant parameters are dielectric constant ($2.2 \leq \varepsilon_r \leq 16$) in RF or micro-wave bands, dielectric loss tangent ($0.0001 \leq \tan\delta \leq 0.06$) or imaginary part of dielectric constant, and expense. Because they have useful surface adhesion, low costs, simplicity of manufacturing, plastics are usually applied in RF and microwave bands, even though that they have weak thermal conductivity, weak dielectric features, large thermal expansion coefficients and weak dimensional stability in comparison to other materials like sapphire and ceramic. The impact of dielectric constant on radiation properties is an additional concern when selecting substrate material. Typically, high dielectric constant lead to low-radiation from microstrip patch antennas [7].

The preferred substrates for optimum performance of antennas are the substrates of high thickness whose dielectric constant is in the range's lower end since they offer improved effectiveness, greater bandwidth, loosely bound fields for radiation to space, but then again at the cost of bigger element size. Microwave circuitry use thin substrates with higher dielectric constants since they need tightly bound fields for minimizing unwanted coupling and radiation, and result in smaller element size; nevertheless, due to their bigger losses, they are less effective and have fairly lesser bandwidth. As MSAs are frequently integrated with other microwave circuitry, cooperation should be achieved between circuit design and the performance of antennas [6].

2.2.4 Fringing Effects of Rectangular Patch

Since the patch dimensions are considered finite along the width and the length, fringing will be done on fields at the patch edges. This will be displayed along the length in Fig (2.1) for the 2 radiating slots of MSA. The same applies along the width.

The fringing amount can be considered as a function associated with the substrate height and patch dimensions. Regarding principal *E*-plane (*xy*-plane) fringing is a function related to the patch width ratio *W* to substrate height *h* (*W/h*) and the substrate dielectric constant ε_r. Because for the MSAs $W/h >> 1$, fringing is going to be reduced; nevertheless, it should be considered since it impacts the antenna's resonant frequency. The same applies for the width [6].

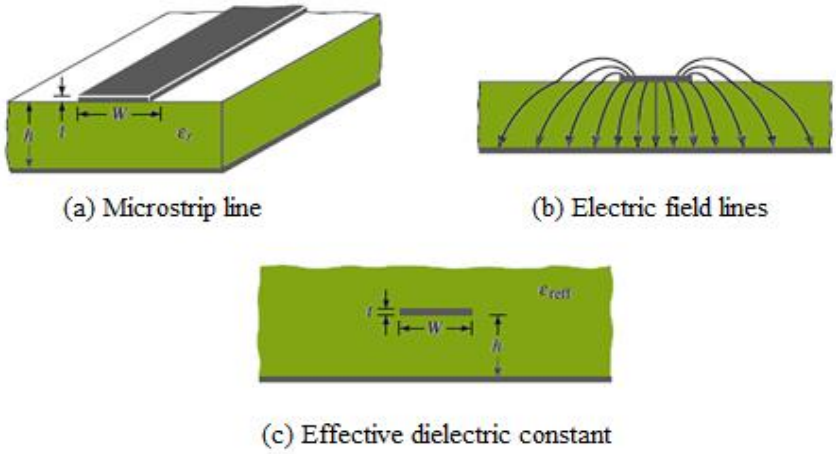

Figure 2.3: Microstrip line and its electric field lines, and effective dielectric constant geometry [6].

For the micro-strip line displayed in Figure 2.3(a), standard electric field lines will be displayed in Figure 2.3(b). This can be defined as a non-homogeneous line of 2 dielectrics; usually air and substrate. As shown, the majority of electric field lines reside in substrates and portions of some lines are existing in air. Since $\varepsilon_r >> 1$ and $W/h >> 1$, electric field lines are mainly concentrated in substrates. In such situations, fringing make the microstrip line seem to be wider electrically in comparison to its physical dimensions. In view of the fact that some waves move in air and some in substrate, *effective dielectric constant* (ε_{reff}) is presented to be responsible for the fringing and wave propagation in the line.

For the purpose of introducing effective dielectric constant, an assumption is made that the central conductor which is related to the micro-strip line with its initial dimensions and height above the ground plane is included in single dielectric, as displayed in Fig (2.3(c)).

The *effective dielectric constant* can be described as the dielectric constant related to uniform dielectric material in order for the line in Figure 2.3(c) to have matching electrical properties, specifically the propagation constant, as the actual line in Figure 2.3(a).

For a line with air that is above substrate, the values of effective dielectric constant are in the range of $1 < \varepsilon_{reff} < \varepsilon_r$. For the majority of implementations in which the substrate's dielectric constant is larger than the unity ($\varepsilon_r >> 1$), ε_{reff} value is going to be closer to the value of real dielectric constant ε_r of the substrate.

Effective dielectric constant can be defined as a frequency function. With the increase of operation frequency, the majority of electric field lines will be concentrated in substrate. Thus; the behavior of micro-strip line will be like a homogeneous line regarding one dielectric (just the substrate), also the effective dielectric constant approaches the value of dielectric constant that is related to substrate. Initial values (at low-frequency) regarding the effective dielectric constant are known as *static values*, for w/h > 1, they are expressed as below:

$$\varepsilon_{reff} = \frac{\varepsilon_r + 1}{2} + \frac{\varepsilon_r - 1}{2}[1 + 12\frac{h}{W}]^{-1/2} \tag{2.1}$$

2.2.5 Effective Length, Resonant Frequency, and Effective Width

Due o the fringing effects, electrically the patch of MSAs appears to be bigger compared to its physical dimensions. Regarding principal *E*-plane (*xy*-plane), which has been displayed in Fig (2.4) in which the patch dimensions along its length were extended on every end via distance Δ*L*, that is considered as a function of effective dielectric constant ε_{reff} and width-to-height ratio (*W/h*).

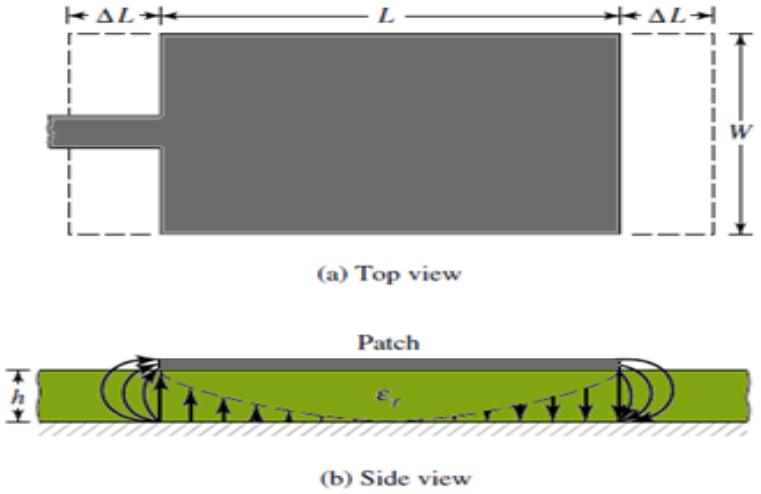

Figure 2.4: Physical and effective lengths of rectangular microstrip patch [6].

The equation below provide a useful and common approximate relation for normalized extension related to length [6]:

$$\frac{\Delta L}{h} = 0.412\frac{(\varepsilon_{reff} + 0.3)(\frac{W}{h} + 0.246)}{(\varepsilon_{reff} - 0.258)(\frac{W}{h} + 0.8)} \tag{2.2}$$

As the patch length was extended via ΔL on every side, the patch's effective length is going to be ($L = \lambda/2$ for dominant TM010 mode without any fringing):

$$L_{eff} = L+2\Delta L \tag{2.3}$$

Regarding the dominant TM010 mode, the MSA's resonant frequency can be considered as a function of its length. Typically it is expressed through:

$$(f_r)_{010} = \frac{1}{2L\sqrt{\varepsilon_r}\sqrt{\mu_o\varepsilon_o}} = \frac{c_o}{2L\sqrt{\varepsilon_r}} \tag{2.4}$$

Where c_o can be defined as the speed of light in the free space. As the Eq. (2.4) accounts for no fringing, it should be changed to comprise edge effects and must be estimated through the use of:

$$(f_r)_{010} = \frac{1}{2L_{eff}\sqrt{\varepsilon_{reff}}\sqrt{\mu_o\varepsilon_o}} = \frac{1}{2(L+2\Delta L)\sqrt{\varepsilon_{reff}}\sqrt{\mu_o\varepsilon_o}}$$
$$= q\frac{1}{2L\sqrt{\varepsilon_r}\sqrt{\mu_o\varepsilon_o}} = q\frac{c_o}{2L\sqrt{\varepsilon_r}} \tag{2.5}$$

Where

$$q = \frac{(f_{rc})_{010}}{(f_r)_{010}} \tag{2.6}$$

Q factor will be specified as *fringe factor* (length reduction factor). When the height of substrate is increased, fringing will also increase and result in bigger separations between lower resonant frequencies and the radiating edges.

2.3 FEEDING TECHNIQUES

A lot of approaches could be applied for the purpose of feeding Microstrip patch antenna. There are 2 categories used to classify such approaches: contacting approaches and non-contacting approaches. Concerning the contacting approach, the radiating patch is fed in a direct way with the RF power through the use of a connecting element like micro-strip line. Regarding the non-

contacting approach, power is transferred between the radiating patch and the line of the micro-strip through coupling of electro-magnetic field. The 5 major feed approaches are: proximity coupling (indirect or non-contacting methods), microstrip line, coplanar waveguide (direct or contacting methods), coaxial probe and aperture coupling [4], [9].

2.3.1 Micro-strip Line Feed

The structure of this category of feed methods is depicted in Figure 2.5, where a conducting strip will be connected to the edge of a micro-strip patch in a direct way. The width of the conducting strip is small in comparison to the patch, the benefit of this type of feed is that the feed could be etched on the same substrate for providing planar structure.

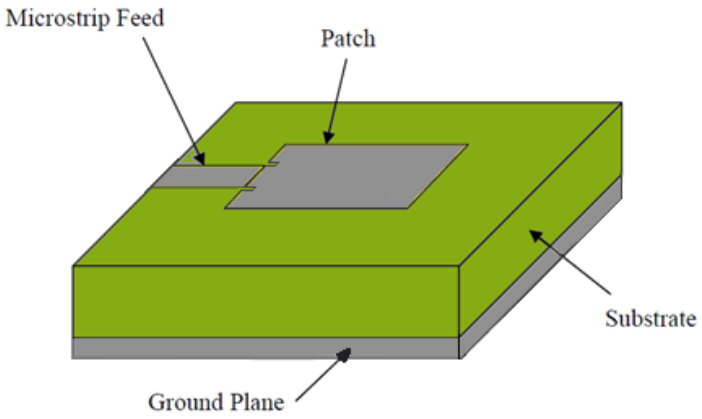

Figure 2.5: Microstrip line feed [6].

The main use of inset cut in the patch is matching the impedance regarding the feed line to the patch with no necessity for further identical element. This is implemented via the correct control of the inset position. Thus, this can be considered as a simple feeding method, because it offers, impedance matching, ease of modelling and simplicity of fabrication. Nevertheless; spurious feed radiation and surface waves will be increased with the increase in the thickness of dielectric substrate, and that will hamper the antenna's bandwidth. Also, undesirable cross polarized radiation is caused by feed radiation [4], [6].

2.3.2 Coaxial Feed

The coaxial feed (which is referred to as probe feed as well) can be considered considered as a usual methods applied to feed micro-strip patch antenna. As depicted in Figure 2.6, the inner conductor that is related to the coaxial connector extend via the dielectric, also it is soldered to the radiating patch, whereas the exterior conductor will be connected to the ground plane, as shown in Figure (2.6) [6].

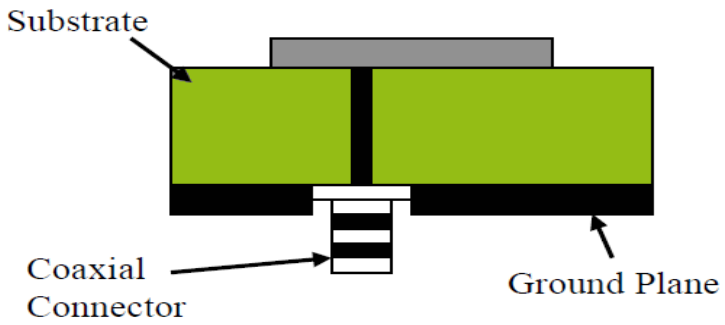

Figure 2.6: Coaxial probe feed [5].

The major benefit of coaxial feed lies in the fact that the feed could be located at any of the chosen locations in the patch in order to match with its input impedance. Coaxial feed has low spurious radiation and it is simple to be fabricated. Yet, the main drawback of this method lies in the fact that it provides small bandwidth, also it is not easy to be modeled due to the fact that a hole must be drilled in the substrate and the connector protrudes outside ground plane, therefore not making it entirely planar for thick substrates ($h > 0.02\ \lambda_o$). Correspondingly, for substrates of higher thickness, increased probe length make input impedance of higher inductivity, resulting in matching issues [4].

As displayed above that for dielectric substrates of high thickness, that offers broad bandwidth, coaxial feed and microstrip line feed experience many drawbacks. These problems will be solved in the following non-contacting feed approaches.

2.3.3 Aperture Coupled Feed

In this approach, the feed line of the micro-strip and radiating patch are separated via ground plane as displayed in Figure 2.7. Coupling between the feed line and the patch is achieved via a slot or aperture in the ground plane.

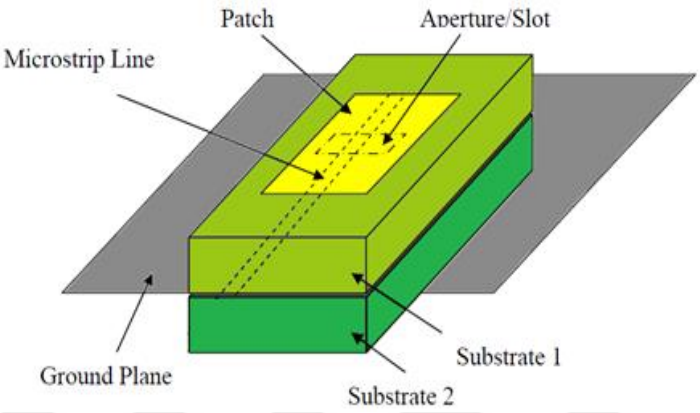

Figure 2.7: Aperture-coupled feed [5].

Usually, a coupling aperture is positioned under the patch, resulting in lower cross polarization because of the symmetry of configuration. The location, size and shape of aperture determines the amount of coupling between the feed line and the patch. Spurious radiation will be minimized as the feed line and patch are separated via ground plane. Normally, high-dielectric material will be deployed for the bottom substrates and low-dielectric constant materials of high thickness will be utilized for top substrates for optimizing the radiation from the patch. The main issue with this method lies in the fact that it is not easy to be fabricated due to the multiple layers, and that will increase the thickness of the antenna. Also, narrow bandwidth is provided by this method [4], [6].

2.3.4 Proximity Coupled Feed

This approach of feeding, which is referred to as electro-magnetic coupling method as well, is depicted in Figure 2.8. Two dielectric substrates have been utilized in this in a way that the radiating patch is on the top of upper substrate and the feed line is between the 2 substrates. The main benefit of this approach is in the fact that it removes spurious feed radiation and it offers quite high-bandwidth, due to the total increasing in the thickness of micro-strip patch antennas.

Also, this approach offers a selections between 2 dielectric media, one for feed line and the other for the patch for optimizing the individual performances [4].

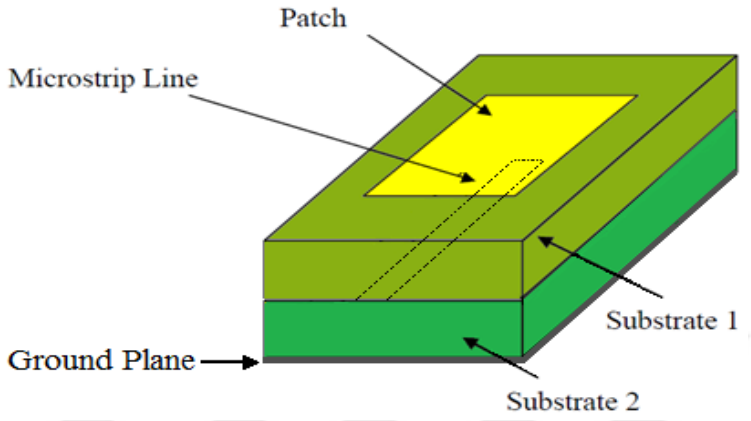

Figure 2.8: Proximity-coupled feed [6].

Matching could be accomplished via controlling width-to-length ratio regarding the patch and the feed line length. The main drawback with this approach lies in the fact that it is not easy to be fabricated due to the 2 dielectric layers that require correct alignment. Correspondingly, the antenna's total thickness will be increased [4].

2.3.5 Co-planar Waveguide (CPW) Feed

Figure (2.9) shows the structure of the coplanar waveguide feed which has been applied to excite the Microstrip antennas. In this approach, the CPW will be etched on the ground plane regarding the Microstrip antenna. The line will be excited through coaxial feed and will be ended via a slot, whose length is going to be selected between 0.25 and 0.29 of the wavelength of the slot. The major drawback of this approach is high radiation from longer slot, resulting in weak front-to back ratio.

Front-to-back ratio will be enhanced through decreasing the dimension of the slot and changing its shape in the form of a loop [4].

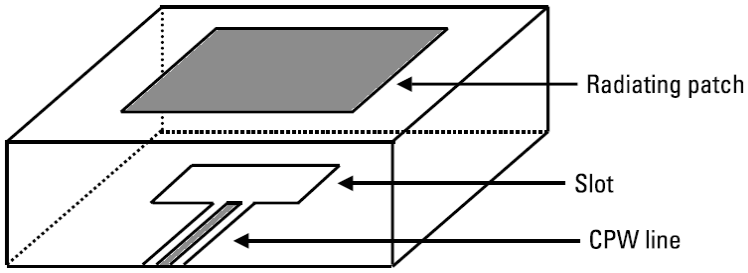

Figure 2.9: Coplanar feed [4].

In summary, Table 2.1 presents a comparative demonstration for the previously described feeding techniques.

Table 2.1: Comparison among the various feeding methods [4], [5].

Properties	Aperture Coupled Feed	Proximity Coupled Feed	Microstrip Line Feed	Coaxial Feed
Spurious Feed Radiation	Less	Lowest	High	High
Reliability	Decent	Decent	Better	Bad because of soldering
Simplicity of Fabrication	Alignment needed	Alignment needed	Simple	Drilling and soldering is required
Impedance Matching	Simple	Simple	Simple	Simple
Bandwidth (accomplished with impedance matching)	2-5 %	13 %	2-5 %	2-5 %

3. APPLICATION OF FRACTAL GEOMETRY IN SLOT ANTENNA DESIGN

3.1 INTRODUCTION

In this chapter, the unique characteristics of fractal geometries will be presented together with the most commonly used fractal geometries applied in the slot antenna design. Regarding this subject, the application related to fractal geometries in slot antenna design could be grouped into 2 types. In the first category, the fractal geometry is applied directly such that it constitutes the whole slot structure, while in the second one; the fractal geometry is applied indirectly. In this case, there is a slot structure with Euclidean shape, such as triangle, square…etc., and fractal geometry has to replace each line segment in this structure.

3.2 FRACTAL PROPERTIES

Fractal indicates irregular or broken fragments; the term fractal has been initially presented through Mandelbrot [10] for describing a family of complex shapes which have non-integer dimension and have inherent self-similarity in their geometrical structures. Which is why, there is a necessity for a geometry which is capable of handling such complicated shapes more efficiently compared to the Euclidean geometry, which has dimensions of integer number, like 1-D line, or 2-D planes...and so on.

Many fields of engineering and science use fractal geometry. A major area of fractal is its use in the antenna design for producing multiband and compact antennas taking advantage of their exceptional features such as self-similarity and space filling [11].

Fractal shaped antennas show certain promising properties, which are associated with their geometrical characteristics. Generally, the fractal structures are composed of multiple copies of themselves at various scales and the fractal's size is defined through the iteration number and the initiator. The fractal, that is utilized in designing antennas, is typically quasi-fractal or pre-fractal yet not mathematically fractal geometry with infinite scale. Thus, quasi- fractal of many iterations could be used for certain multi-band antennas. All frequency bands are conforming to a certain fractal's scale [12].

Fractal antenna engineering can be defined as a developing field which uses the concepts of fractal to develop novel antenna types with distinguished properties. The self-similarity related to fractal structures cause antenna' multiband behavior and frequency-selective surfaces. On the other hand, the space-filling properties lead to miniaturized and compact size antennas. Recently, extensive studies were focused on fractal antenna engineering. Fractal methods were utilized to loops, monopoles, patches, dipoles, and slot antennas [13].

3.2.1 Space-Filling

Fractal curves can be distinguished through a special feature that, following infinite iterations, their length become infinite even though the whole curve fit into finite area as shown in Figure (3.1). Such feature could be used for miniaturization of microstrip and printed antennas through increasing the effective electrical length via which current travels. Many applications can benefit from fractal antennas. The continuous development in the field of wireless communication has increased the necessity for compact integrated antennas. Space saving capabilities which are related to fractals to effectively fill a small amount of space provide special benefit of applying integrated fractal antennas over Euclidean geometry [14]

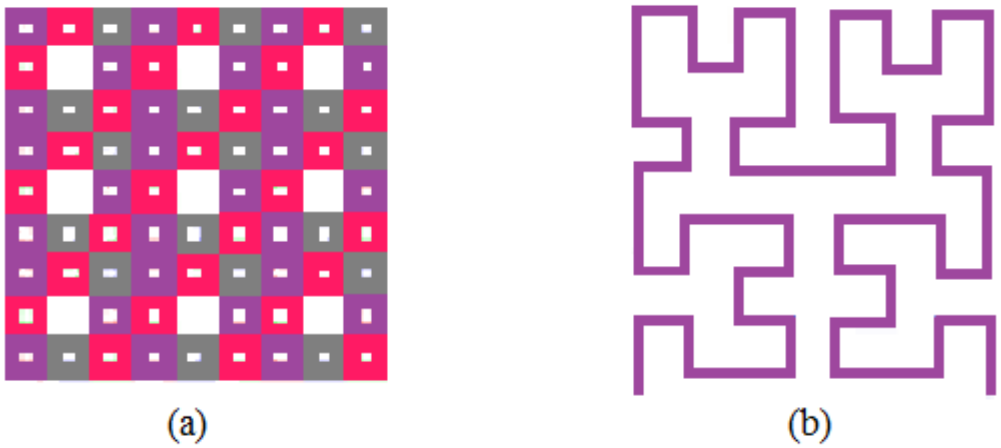

Figure 3.1: Space-filling fractals of (a) 3rd iteration Sierpinski carpet, and (b) 3rd iteration Hilbert curve [15], [16].

3.2.2 Self-Similarity

Self-similarity property means that a small part of the structure is a scaled-down copy of the original structure, as displayed in Figure (3.2). Therefore, antennas can operate at multiple frequency bands. Traditional fractal geometries including Minkowski, Cantor, Koch, Sierpinski, Hilbert, and other fractal curves were efficiently utilized for producing multi and dual band printed slot antennas for many wireless applications [17].

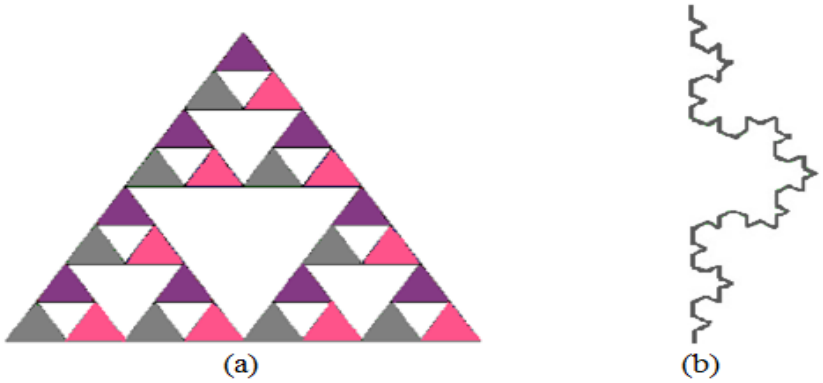

Figure 3.2: Self- similar fractals of (a) 3rd iteration Sierpinski gasket, and (b) 3rd iteration Koch curve [15].

3.2.3 Fractal Dimension

The main feature of fractals is that they have non-integer dimensions dissimilar to the Euclidian which have integer dimensions. The common intuitive concept of dimension is called the topological dimension. A cube, line segment, point and a square, as displayed in Figure (3.3) have topological dimensions of 0, 1, 2 and 3, respectively. An integer number is always used for expressing the intuitive dimension [18].

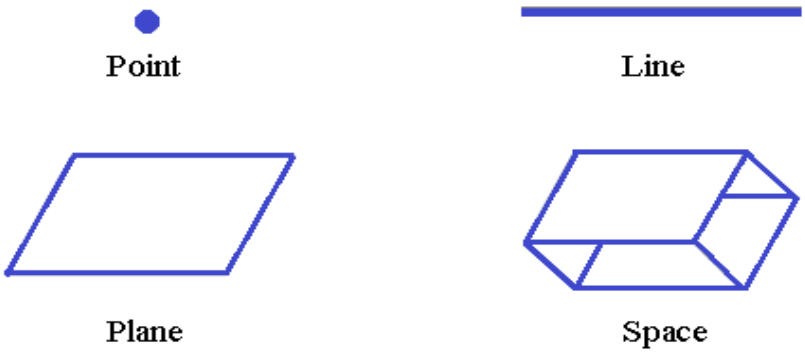

Figure 3.3: Euclidean geometries [14].

Fractal dimension is associated to the self-similarity in that the simplest method for creating a figure that has fractal dimension by self- similarity. Then, the fractal dimensions (FD) will be, as given by [14]:

$$FD = \frac{\log_{10}(N)}{\log_{10}(1/r)} \qquad (3.1)$$

Where N can be defined as the overall number of distinct copies, r can be defined as the reduction factor value that indicates how will be the new side length regarding the original side length. In order to calculate the fractal dimension of any self-similar shape, the shape can be split into N parts, where the size of each part is related to the size of the original one by the reduction factor value. The fractal dimension FD equals the topological dimension for any Euclidean shape, but FD can also be evaluated for any non-standard shapes that exhibit self-similarity [19].

Dimension of some geometrical shapes are listed below in Table (3.1). The fourth column contains the FD value for each shape, where FD is calculated using equation (3.1). Figure (3.4) demonstrates Euclidean geometrical shapes which are split into N parts by using a reduction factor of 1/2 to divide a line segment, square and cube [20].

Table 3.1: Dimensions of geometrical shapes

Shape Name	*r*	N	FD
Line	½	2	1
Square	½	4	2
Cube	½	8	3
Cantor Set	1/3	2	0.63
Sierpinski Gasket	½	3	1.58
Minkowski Island	1/3	5	1.46

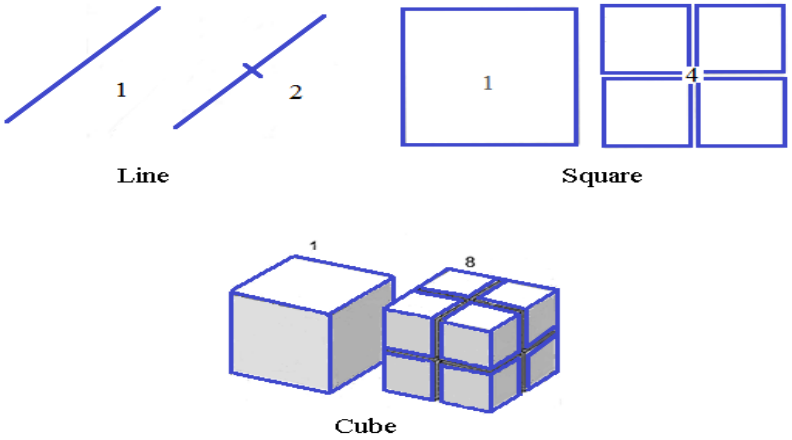

Figure 3.4: Euclidian geometrical shapes with a reduction [15].

3.3 FEATURES AND LIMITATIONS OF FRACTAL GEOMETRIES IN ANTENNA DESIGN

Features:

- Miniaturization.
- More efficient input impedance matching multi and wide bands (utilizing single antenna rather than several).
- Decreased mutual coupling in the fractal array antennas
- Frequency independent (reliable operation throughout large ranges of frequency).

Limitations:

- Complexity (some types are complex to construct).
- Numerical limitations (become less with the continuing advance in computer technologies).
- The benefit begins to diminish after first few iterations.

However, the features offered by the fractal geometries are more than limitations that they have encountered. In addition, the advances in computer technologies and the computational techniques have contributed to make these limitations less important [21].

3.4 COMMONLY USED FRACTAL GEOMETRIES IN ANTENNA DESIGN

Large number of fractal geometries and their variants are reported in the literatures [10], [14], [19], but very limited number among these were adopted in designing antennas for various applications. In the following subsections, a presentation of the most commonly used fractal types.

3.4.1 Cantor Set

Cantor set can be defined as a standard fractal object that displays precise self-similarity through all scales [14].

Cantor set include infinite set related to the disappearing segments of the line in unit interval. The optimal way for understanding Cantor set fractal is displaying its construction approach, as shown in Figure (3.5) for the plainest type of Cantor set (the triadic Cantor set).

The set will be created via eliminating the middle third of unit line segment (step k = 1 in figure). From the two segments that remained of the line, every one of which is 1/3 in length, middle thirds will be removed once more (step k = 2 in the figure). Middle thirds of the 4 of the rest of line segments, every one of which is 1/9 in length, will afterwards be eliminated (k = 3) and similarly to infinity. The remaining is considered as a set of infinitely various disappearing segments of the line that lie on unit interval whose combined and individual lengths come close to 0. Such point set is referred to as Cantor dust or Cantor set [22].

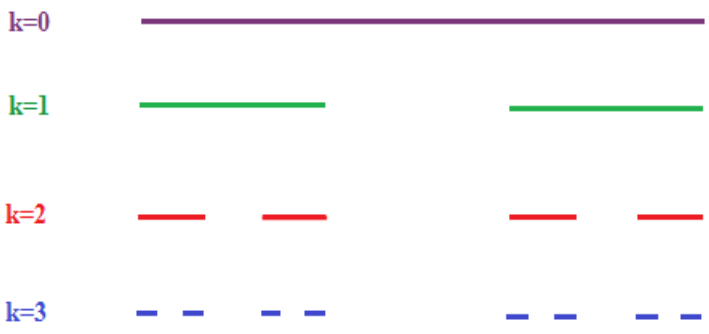

Figure 3.5: The generation of Cantor set [14].

Regarding the Cantor set construction, the initial unit line segment $k = 0$, is referred to as the set's initiator. The initial stage, $k = 1$, is referred to as the generator or motif, since it is considered as the repeated iteration related to this stage on the following line segment that result in the set's creation. It is necessary repeating the generation procedure only via the number of stages needed to deceive the eye, and not countless times (which is considered accurate for every illustration that is related to fractal objects). Yet, the Cantor set is obtained following infinite number of iterations. A set of line segments with a particular measurable length are produced via a finite number of iterations. Such objects created *en route* to fractal object are referred to as pre-fractals [23].

3.4.2 Koch Curve

This construction method is displayed in Figure (3.6), it is considered as an extra sufficiently documented fractal. Just like the Cantor set, Koch curve is easy to construct through the use of iterative process starting with set's initiator as the unit line segment (stage $k = 0$ in figure). The unit line segment will be separated to thirds, the middle one will be eliminated. After that, the middle third will be substituted by 2 equal parts, they two are 1/3 in length, that create an equilateral triangle (stage $k = 1$): this stage is the curve generator. In the following stage ($k = 2$), the middle third will be eliminated from the 4 segments, every one of which will be substituted by 2 equal segments. Koch curve will be produced after repeating this procedure for an infinite number of times. Once more, the set's self-similarity is obvious: all sub-segments are considered as carbon copy of the original curve, as displayed in Fig. (3.6) [24].

A visible feature of Koch curve is that it apparently has an infinite length. Which could be visible from the process of construction. At every stage, k, in its generation, the length regarding the pre-fractal curve will increase to L_{k-1}, where L_{k-1} can be defined as the length of the curve in the previous stage.

It might be visible that Koch curve is efficiently produced from corners, thus, there is no unique tangent happens upon it. Koch curve isn't a smooth, also it is nowhere-differentiable, as unique tangent, or slope, cannot be found upon it. It is a fractal object that possesses a fractal dimension. Every one of the smaller segments of the Koch curve is a precise simulation of the entire curve [25].

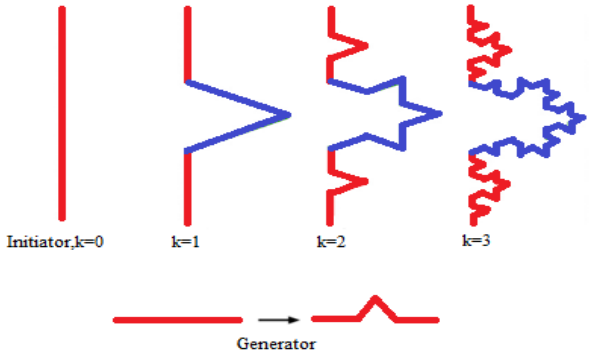

Figure 3.6: The generation of Koch curve [25].

3.4.3 Sierpinski Gasket and Carpet

The construction which is related to Sierpinski gasket is displayed in Fig. (3.7). Filled triangle in the plane is the initiator in such case. The middle triangular part will be eliminated from original triangle. After that, the central triangular segments will be eliminated from the rest of the triangular elements etc. Sierpinski gasket is created following an infinite number if iterations. All pre-fractal step in construction are composed of 3 smaller copies of the previous step, every one of the copies is scaled through a factor of 1/2 [26].

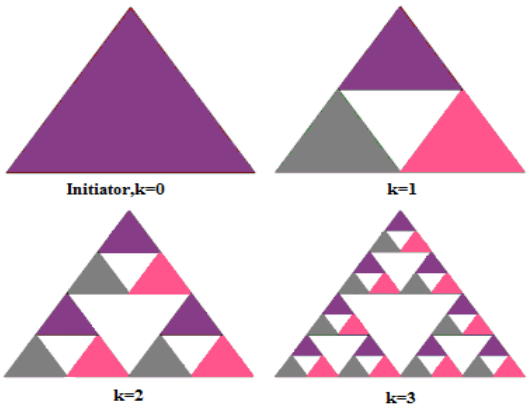

Figure 3.7: The generation of Sierpinski gasket [26].

Sierpinski carpet is another variant of Sierpinski gasket, it is displayed in Fig. (3.8). The construction approach for gasket and carpet are similar. In this case, the initiator is a square and the generator will remove the central square, that its side length 1/3 of the original square. With Sierpinski carpet and gasket, the constructions cause fractal curves whose area vanishes [27].

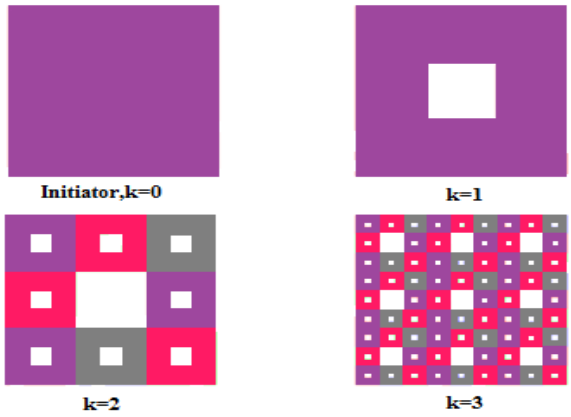

Figure 3.8: Generation of Sierpinski carpet [27].

3.4.4 Minkowski Island Fractal

The starting geometry regarding Minkowski island fractal, referred to as initiator, is a Euclidean square. All the 4 straight segments related to the starting structure will be substituted by generator, which has been displayed at the bottom of Fig. (3.9). This iterative generating process will continue for infinite times. The ultimate outcome is a curve with infinitely intricate underlying structure which is not differentiable at any point. The generator will replace all straight segments of geometry. The initiator is square as displayed in the Figure (3.9) along with the first three construction iterations [28].

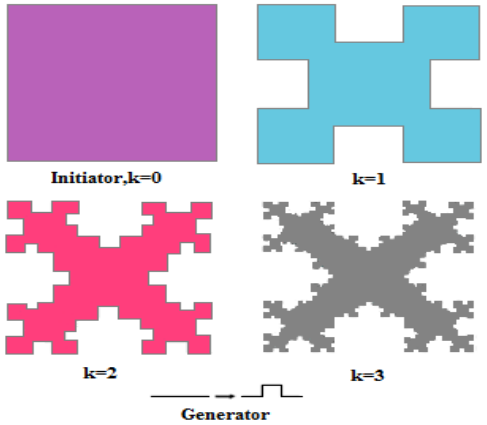

Figure 3.9: The generation of Minkowski island fractal [28].

3.4.5 Hilbert Curve

The first four iterations with initiator of Hilbert curves are displayed in Figure (3.10). It could be noticed that the geometry at a step could be acquired by putting together 4 copies of the preceding

iteration, linked to additional line segments. A lot of Hilbert pre-fractal based structures were suggested for producing printed and micro-strip dipole and monopole antennas with compact size and multi-band performance for various implementations [29]

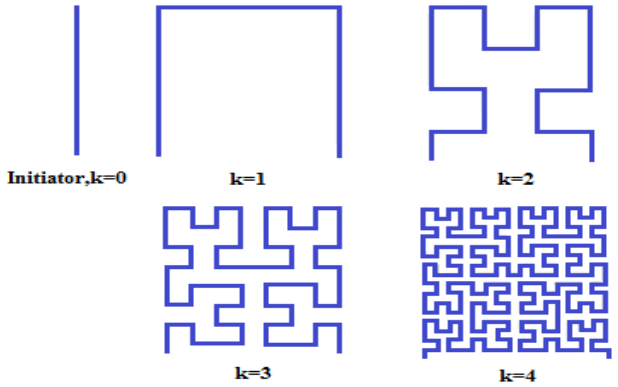

Figure 3.10: The generation of Hilbert curve [29].

3.4.6 Peano Curve

The initiator regarding Peano curve is again specified via a straight line and the correspondent generator include 9 lines one-third of initiator. The first generator's line runs horizontally, the second turns up 90 degrees, after that, a horizontal segment follows prior to when the curve turns down by 90°. The fifth line move back to the end of the first line with no touching between them. The following part of the curve heads down by 90 degrees, followed by a horizontal part prior to the time where it goes up again. Finally a line located in horizontal position once more forms the last part, as shown in Figure (3.11) .This type is used in antenna design as a modified structure in [30].

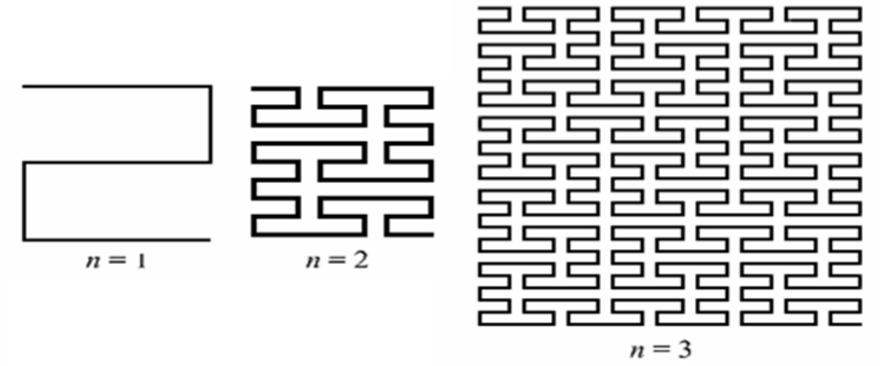

Figure 3.11: The first three iterations levels to construct the Peano pre-fractal curve [30].

4. DESIGN AND RESULTS

4.1 INTRODUCTION

In this chapter, two microstrip antennas based on quasi fractal geometries have been simulated by using Applied Wave Research (AWR). On the hand, one printed slot antenna based on slotting the ground plane with stair step structure has designed, modeled, fabricated and their characteristics' performance are assessed [31].

4.2 QUASI FRACTAL ANTENNAS

The expansion of wireless systems has been developed the notion of a structural antenna design where the end-devices relay signals with electromagnetic access are joined with a dominant network server in the backend. The communication among end-devices and gateway is typically wireless communication within RF or microwave band frequencies. In this study, a small antenna size using FR-4 substrate to work in RF or Microwave wireless application is presented. To accomplish the above objectives, microstrip patch antenna with smallness features and quasi fractal shape are used. The simulations were done using Advanced Wave Research (AWR) simulator. The planned antenna is intended to be highly compact that can be integrated within any system or devices with sufficient performances [32].

Microstrip antenna is, in general, has three parts. The upper layer stands for microstrip or transmission line that usually has a thickness (t) of 35 μm with specified topology and dimensions. The intermediate layer is a substrate layer specified by dielectric material with dielectric constant ($\in_r$) and thickness symbolized by h. The most commonly used substrate material is FR4 substrate. The bottom layer is typically conductor ground plane [2, 3].

The top view of the presented microstrip patch antenna has distributed similar slots as clarified in Figure 2. It was modeled by applied wave research (AWR) simulator by assembling uniform regular resonator that is known as quasi-fractal resonator. The AWR simulator has meshing drawer and has possibilities to choose substrate specifications and dimensions as well as operating frequencies. As grid size and step frequency is chosen smaller, accuracy of simulation results with respect to measurements will be increased [33]. The lowest square patch generator viably initiates

the antenna structure as in Figure 4.1. It possesses a length of 2.5 mm while the biggest square patch constituent is 9 mm. The full length of this microstrip quasi-fractal resonator has been 34 mm. Via Ports (1) and (2) as positioned in Figure 2 are adopted for circular polarization. The used substrate material is FR4 substrate with $\in_r = 4.4$ and h=1.6 mm.

An important issue in the smallness of microstrip antennas comes from the actuality that resonating devices have to comprise absolute dimensions related to the guided wavelength, according to evaluated resonant frequency (f). The guided wavelength can be evaluated by:

$$\lambda_g = \frac{c}{f\sqrt{\varepsilon_e}} \tag{4.1}$$

An effective relative dielectric constant ε_e, for the square patch antenna can be computed from Eq. (4) [17], [34], [35]:

$$\varepsilon_e = \frac{\varepsilon_r + 1}{2} + \frac{\varepsilon_r - 1}{2}\left(\frac{1}{\sqrt{1+12H/A}}\right) \tag{4.2}$$

All the same, ε_e in this study has been calculated using the approximated equation that can be adopted in patch antennas as stated in [34]:

$$\varepsilon_e = \frac{\varepsilon_r + 1}{2} \tag{4.3}$$

Relatively, the projected antennas have been designed using a single layer of FR4 substrate with a relative dielectric constant (ε_r) of 4.4 and a substrate height (H) of 1.6 mm.

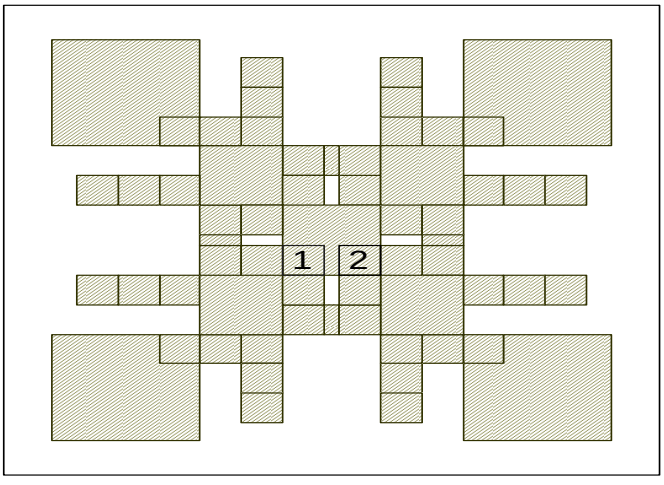

Figure 4.1: Simulated multiband microstrip antenna

Figure 4.2 describes the S11 (input reflection) response of the designed quasi-fractal antenna. It signposts triple frequency performance for the antenna at *2.905* GHz , *3.87*GHz and *5.545* GHz in 1 to 8 GHz frequency full range. All resonances have input reflection of deeper than -10 dB.

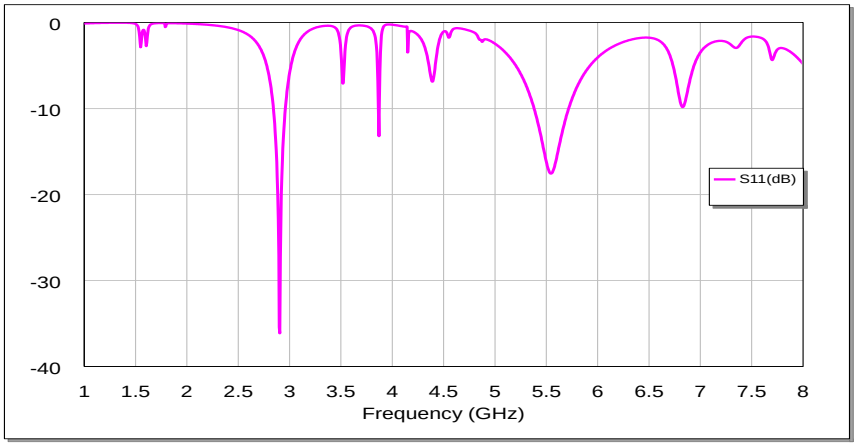

Figure 4.2: Input reflection (S11) response of microstrip quasi-fractal antenna

Figure 4.3 describes the angle or phase response of the simulated antenna. Its results possess various active and linear pathways within 1 to 8 GHz sweeping frequencies.

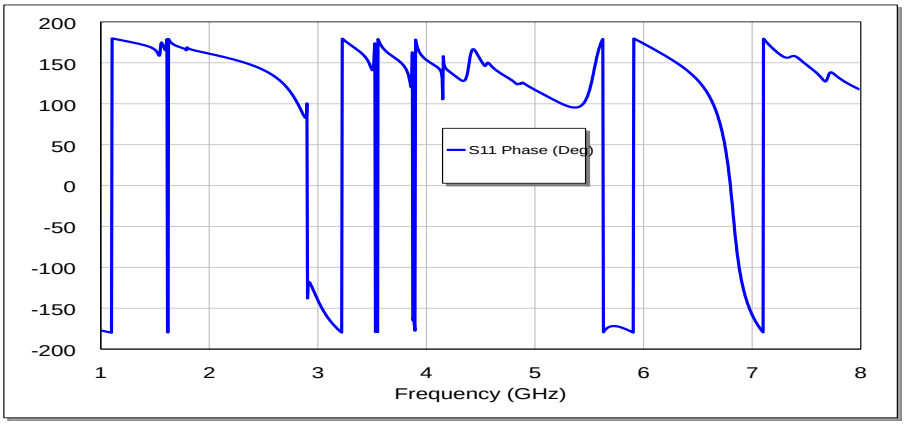

Figure 4.3: The phase response of the suggested antenna

Figure 4.4 displays the group delay of the simulated antenna. It is understandable that there are negative and positive delay values due to the transmission line of the quasi-fractal resonator and resonance modes with akin are potential in microstrip antenna.

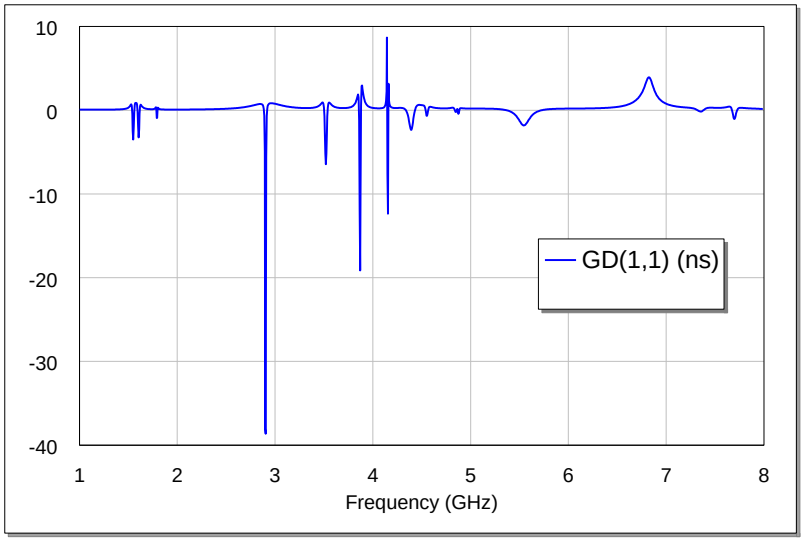

Figure 4.4: The group delay result of suggested microstrip antenna.

Figure 4.5 Figures 4.6 illustrate the PPC-LHCP (principal plane cut left hand circular polarization) and PPC RHCP (principal plane cut right hand circular polarization) respectively at $\varphi = 0\circ$. RHCP and LHCP are determined from the following formulas at their resonant frequencies:

$$RHCP = \frac{E\theta + jE\varphi}{\sqrt{2}} \tag{4.4}$$

and

$$LHCP = \frac{E\theta - jE\varphi}{\sqrt{2}} \tag{4.5}$$

As it can be observed from previous figures, PPC-LHCP and PPC-RHCP responses are within θ sweeping from -90 to 90 degrees at fixed φ and assigned resonant frequency. Each antenna possesses a specific radiation pattern in accordance with resonant frequency in the of PPC-LHCP and PPC-RHCP cases. However, these patterns are tolerable in antenna design theory.

Figures 4.7 describe PPC-TPWR (PPC total power) radiation patterns at φ = 0^o and resonant frequencies. PPC-TPWR represents the available total power from Eφ and Eθ fields regardless of polarization.The resulting PPC-TPWR patterns are satisfactory for first antenna.

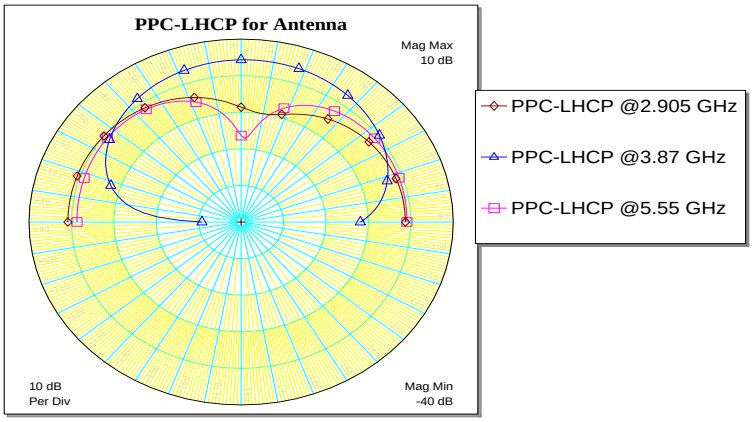

Figure 4.5: PPC-LHCP radiation patterns for First quasi fractal antenna

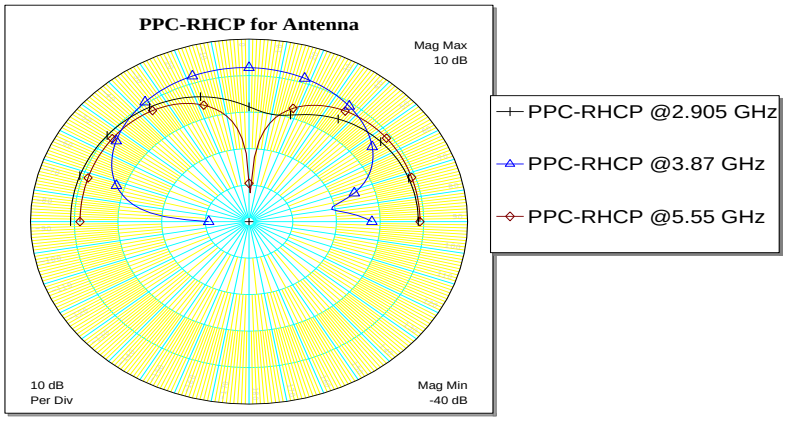

Figure 4.6: PPC-RHCP radiation patterns for First quasi fractal antenna

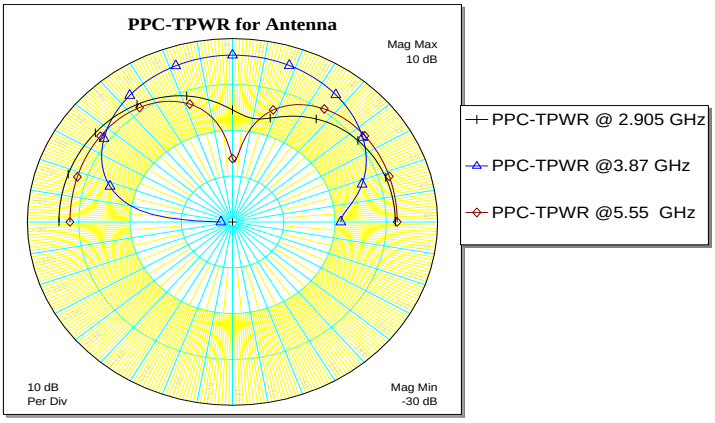

Figure 4.7: PPC-TPWR radiation patterns for First quasi fractal antenna

The top view of the second microstrip patch antenna has distributed analogous slots as clarified in Figure 4.8. It was modeled by applied wave research (AWR) simulator by assembling uniform regular resonator that is known as quasi-fractal resonator. The AWR simulator has meshing drawer and has possibilities to choose substrate specifications and dimensions as well as operating frequencies. As grid size and step frequency is chosen smaller, accuracy of simulation results with respect to measurements will be increased. The lowest square patch generator viably initiates the antenna structure as in Figure 4.8. It possesses a length of 2.5 mm while the biggest square patch constituent is 9 mm. The full length of this microstrip quasi-fractal resonator has been 34 mm. Via Ports (1) and (2) as positioned in Figure 4.8 are adopted for circular polarization. The used substrate material is FR4 substrate with $\in_r = 4.4$ and h=1.6 mm.

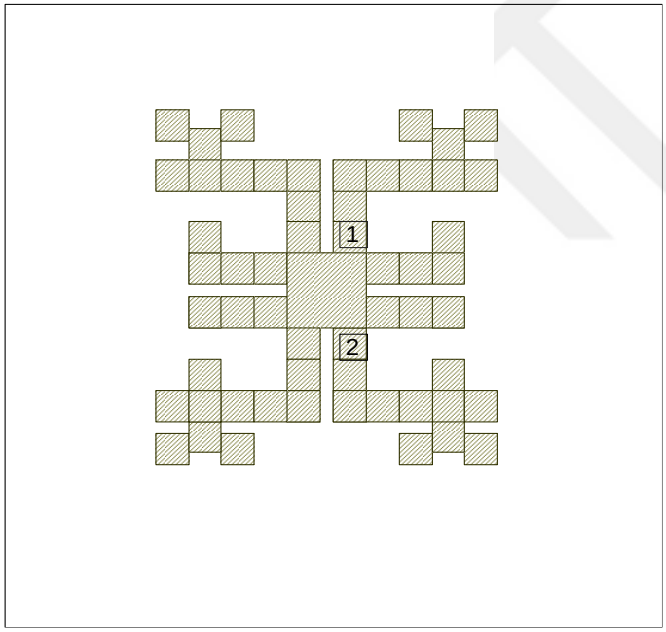

Figure 4.8: Simulated multiband second microstrip antenna

Figure 4.9 describes the S11 (input reflection) response of the designed quasi-fractal antenna. It signposts multi band frequency response for the antenna at 1.537 GHz , 2.643 GHz , 3.368 GHz and 7.589 GHz in 1 to 8 GHz frequency full range. All resonances have input reflection of deeper than -10 dB.

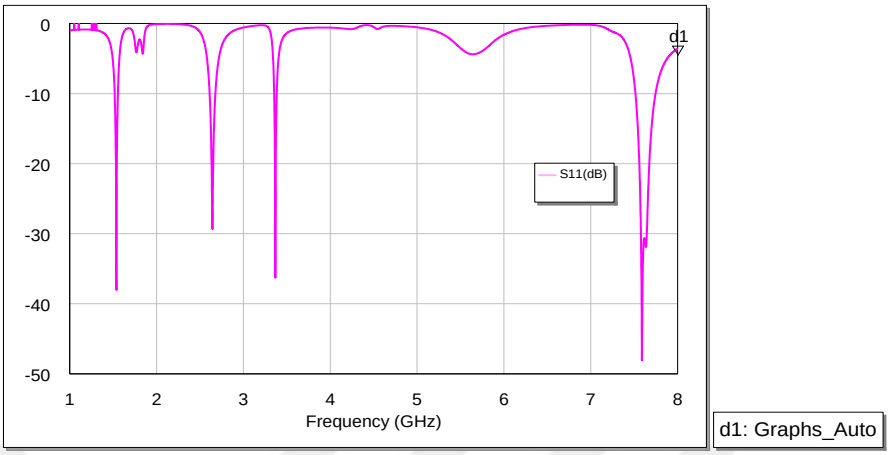

Figure 4.9: Input reflection (S11) response of second microstrip quasi-fractal antenna

Figure 4.10 describes the angle or phase response of the simulated antenna. Its results possess various active and linear pathways within 1 to 8 GHz sweeping frequencies.

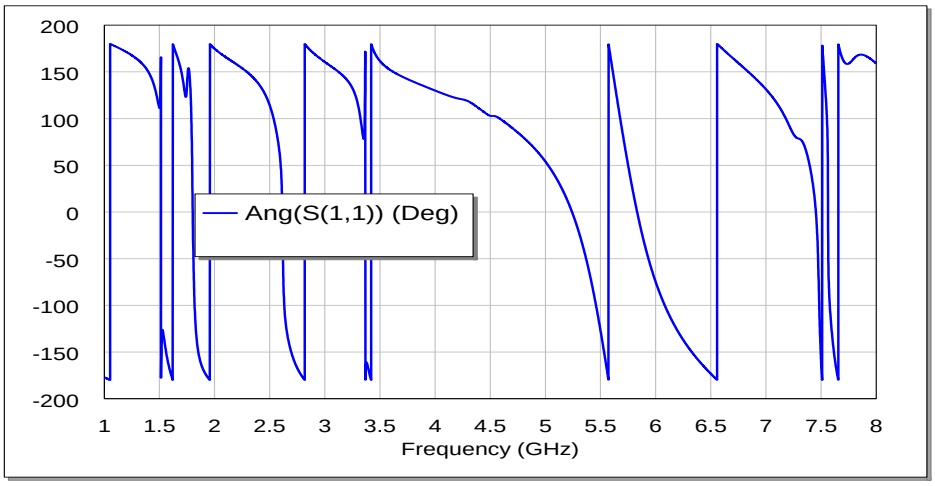

Figure 4.10: The phase response of the second antenna

Figure 4.11 displays the group delay of the simulated antenna. It is understandable that there are negative and positive delay values due to the transmission line of the quasi-fractal resonator and resonance modes with akin are potential in microstrip antenna.

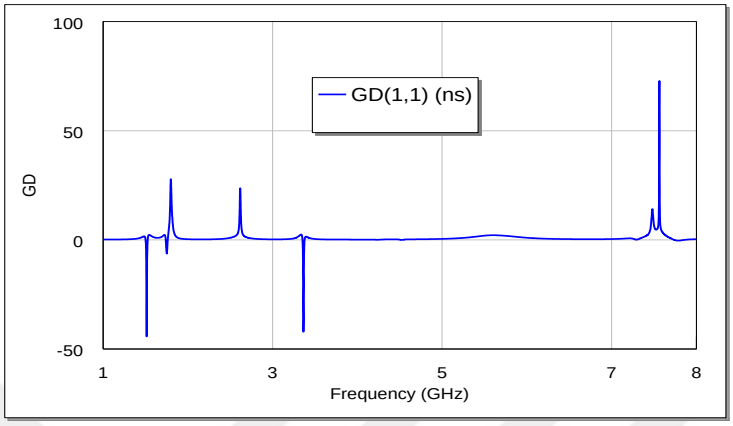

Figure 4.11: The group delay result of second microstrip antenna

Figure 4.12 Figures 4.13 illustrate the PPC-LHCP (principal plane cut left hand circular polarization) and PPC RHCP (principal plane cut right hand circular polarization) respectively at $\varphi = 0\circ$. RHCP and LHCP are determined from the following formulas at their resonant frequencies:

$$RHCP = \frac{E\theta + jE\varphi}{\sqrt{2}}$$

and

$$LHCP = \frac{E\theta - jE\varphi}{\sqrt{2}}$$

As it can be observed from previous figures, PPC-LHCP and PPC-RHCP responses are within θ sweeping from -90 to 90 degrees at fixed φ and assigned resonant frequency. Each antenna possesses a specific radiation pattern in accordance with resonant frequency in the of PPC-LHCP and PPC-RHCP cases. However, these patterns are acceptable in antenna design theory.

Figures 4.14 describe PPC-TPWR (PPC total power) radiation patterns at φ = 0^o and resonant frequencies. PPC-TPWR represents the available total power from Eφ and Eθ fields regardless of polarization.The resulting PPC-TPWR patterns are satisfactory for first antenna.

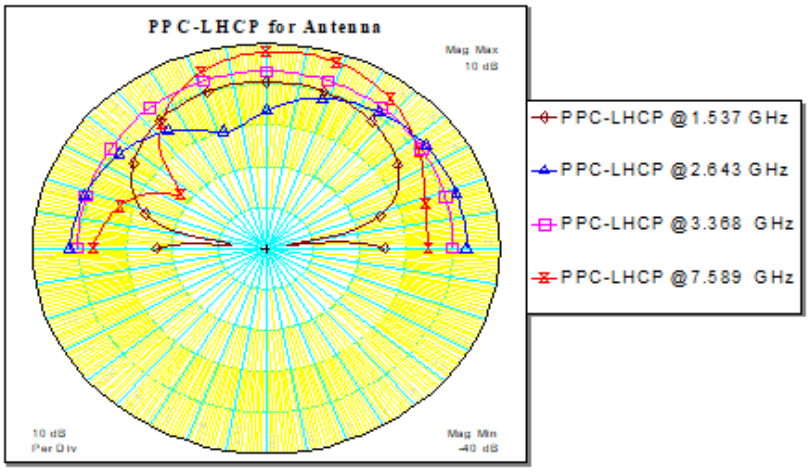

Figure 4.12: PPC-LHCP radiation patterns for second quasi fractal antenna

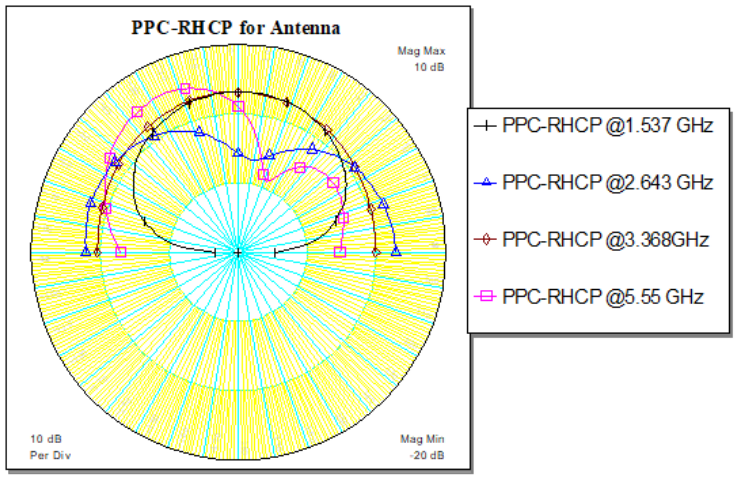

Figure 4.13: PPC-RHCP radiation patterns for second quasi fractal antenna

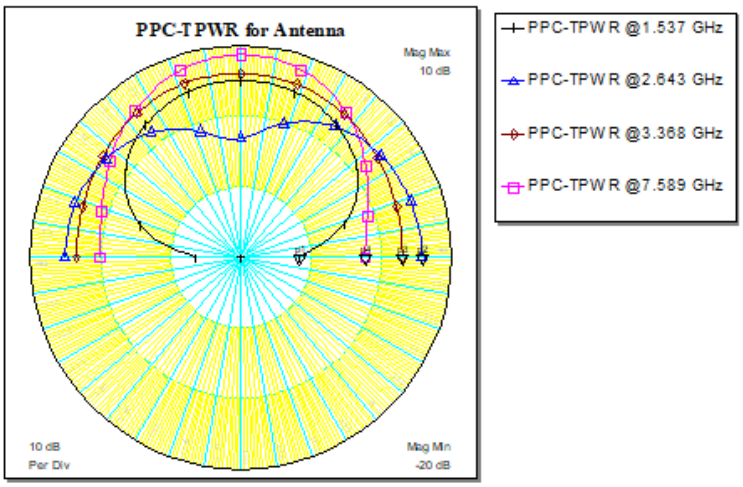

Figure 4.14: PPC-TPWR radiation patterns for second quasi fractal antenna

4.3 PRINTED SLOT ANTENNAS

The third device is printed slot antenna that is with slot structure resulting from the application of printing stair-step slot geometry in the ground. In this section, a printed slot antenna is to be accessible to serve as a candidate in dual wireless band uses and utilizes. Simulation has been done with CST electromagnetic simulator. Its dimension details are illustrated in Table 4.1.

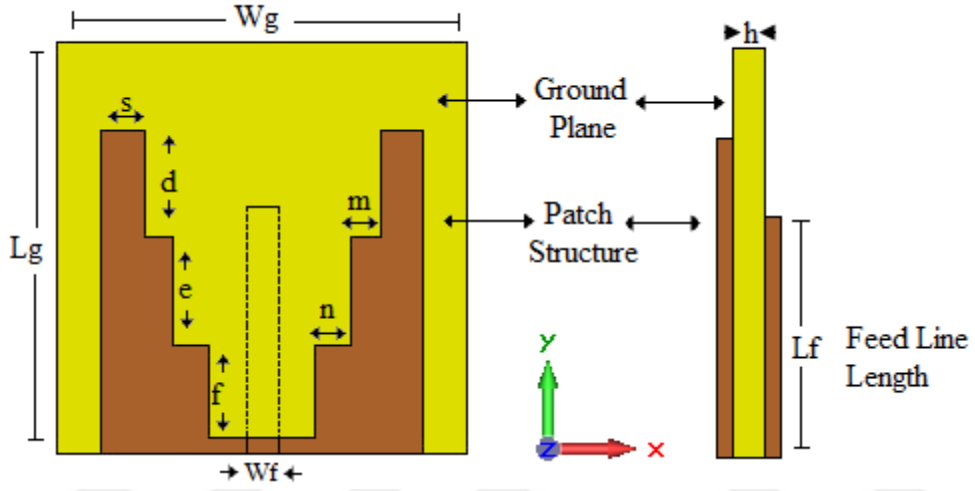

Figure 4.15: Topology of third antenna based on printed slot type

Table 4.1: Dimensions of printed slot antenna

Wg	40mm	f	10.5mm
Lg	40mm	m	2.8mm
S	4.2mm	n	3.5mm
d	10.5mm	Wf	3mm
e	10.5mm	Lf	24mm

Figure 4.16 shows the responses of input reflection of the third antenna along with the feeding line as a parameter within the frequency of sweep of 1 to 10 GHz. For various lengths of the feeding line, the antenna provides responses of S11 response of single and dual band results based on feed length (Lf) ranged from 16 to 26 mm. It is clear that the first resonances have potential lower input

reflection (return loss) than the second resonance. Based on this parametric investigation, we have selected the single band response around 5.75 GHz for investigation, fabrication and measurements as in Figure 4.17.

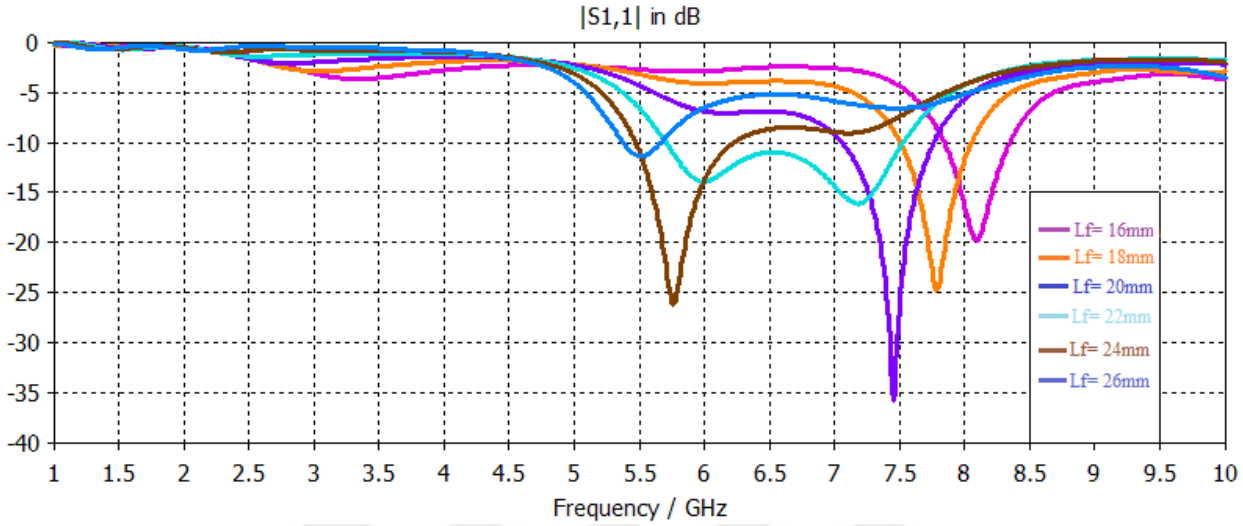

Figure 4.16: s11 responses of third antenna based on feed length from 16 – 26 mm**.**

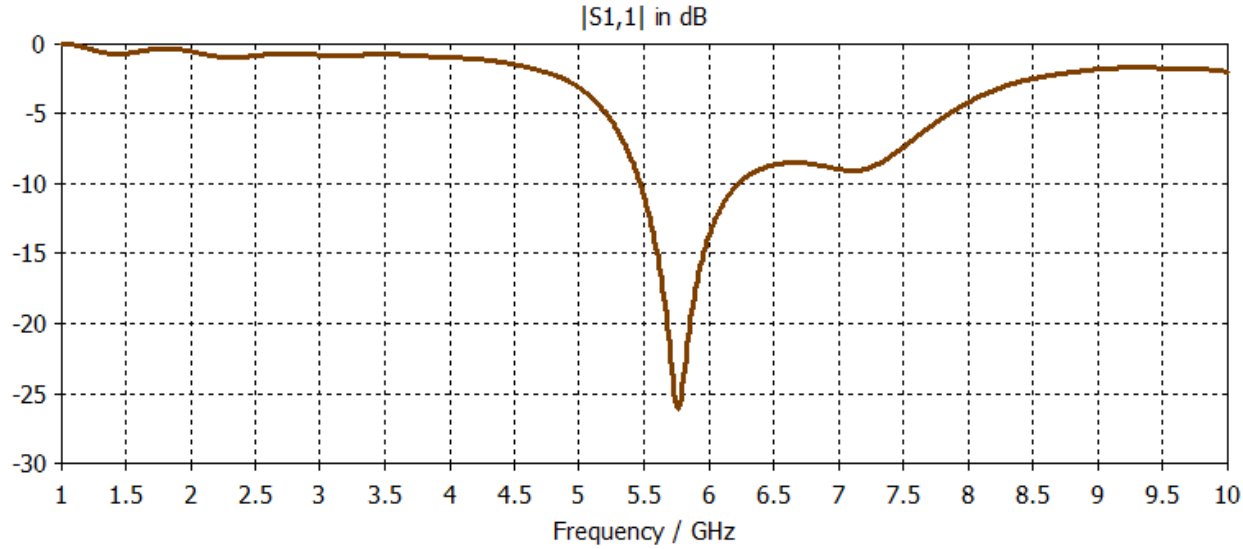

Figure 4.17: S11 responses of third antenna based on feed length of 24 mm

In order to obtain more information about the properties of EM for the third antenna, the current intensity distributions in the antenna have simulated at 5.75 GHz, as shown in Fig. 4.18. As a result of Figure 4.18 indicates, maximum intensities are concentrated nearby feed regions and stair-step edges with value of 32.9 A/m.

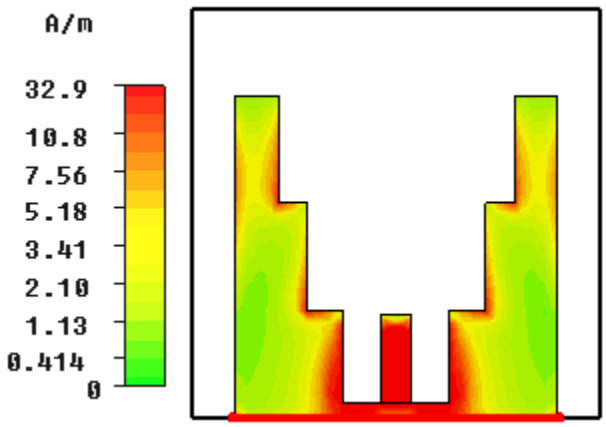

Figure 4.18: current intensity distribution at f=5.75 GHz.

For the characteristics of radiation, Figure 4.19 illustrates the three-dimensional patterns of radiation that simulate the resulting antenna at 5.75 GHz.

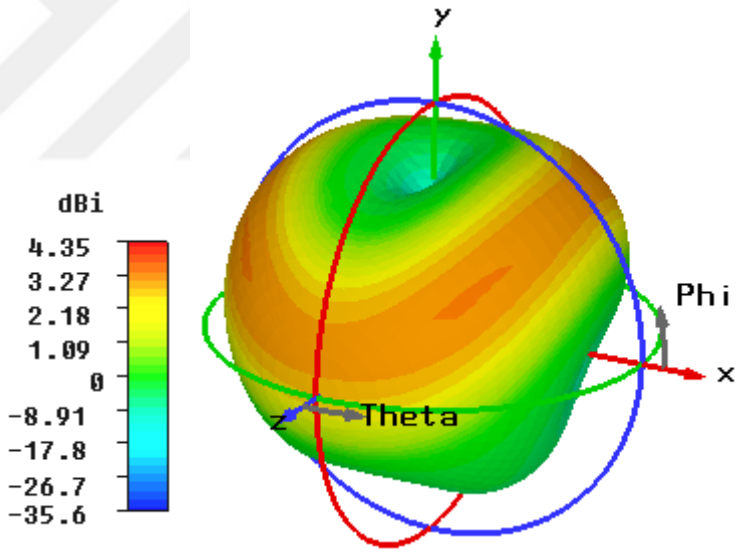

Figure 4.19: directivity of third designed printed slot antenna at f= 5.75GHz**.**

The maximum gains magnitudes were evaluated in the band of 5.75 GHz, as demonstrated in Fig. 4.20. In the frequency of single band, the gains are ranged from 1.8 dBi to less than 2.4 dBi.

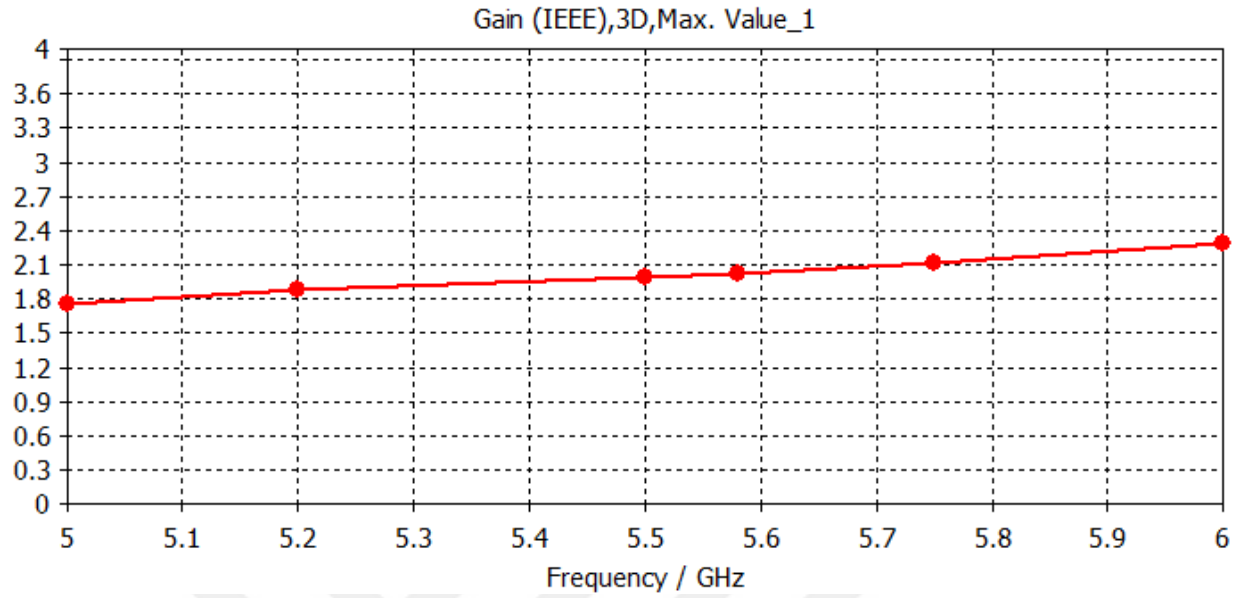

Figure 4.20: Resultant gain with 5-6 GHz range

Figure 4.21 clarifies the simulating long–distance patterns' radiation for the whole field of electric in the x-y, x-z, and the y-z planes at 5.75 GHz.

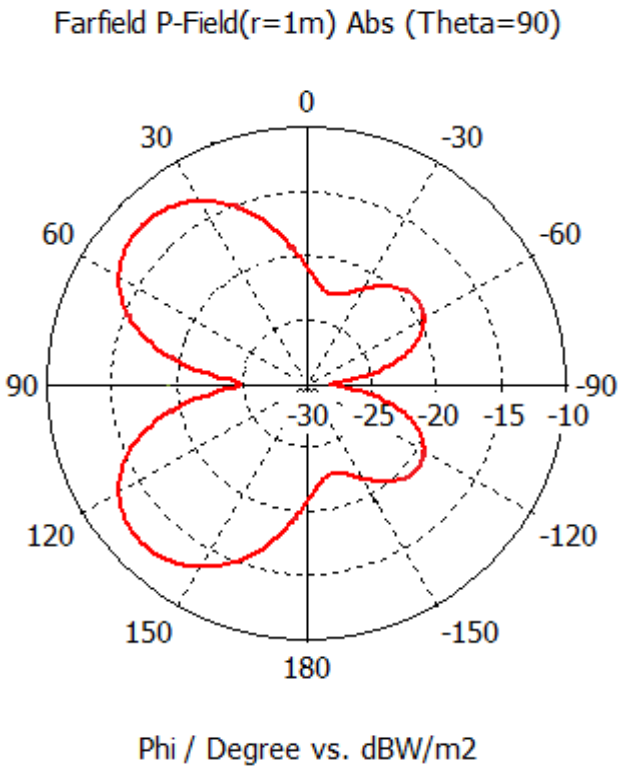

(a) xy-plane (f=5.75 GHz)

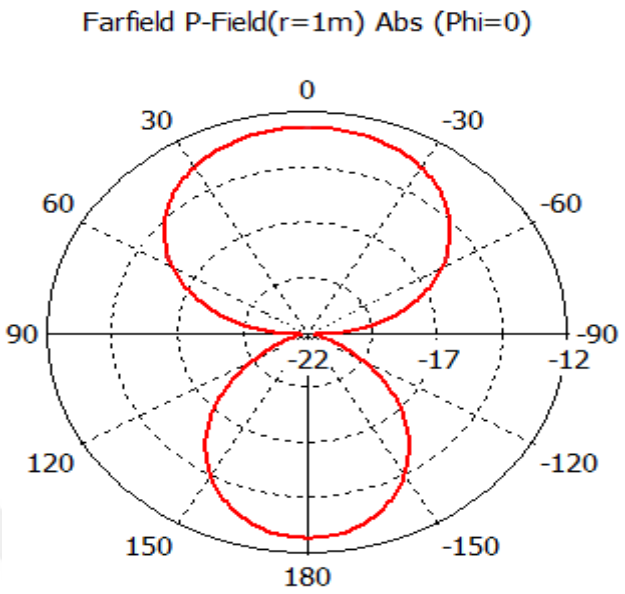

(b) xz-plane (f=5.75 GHz)

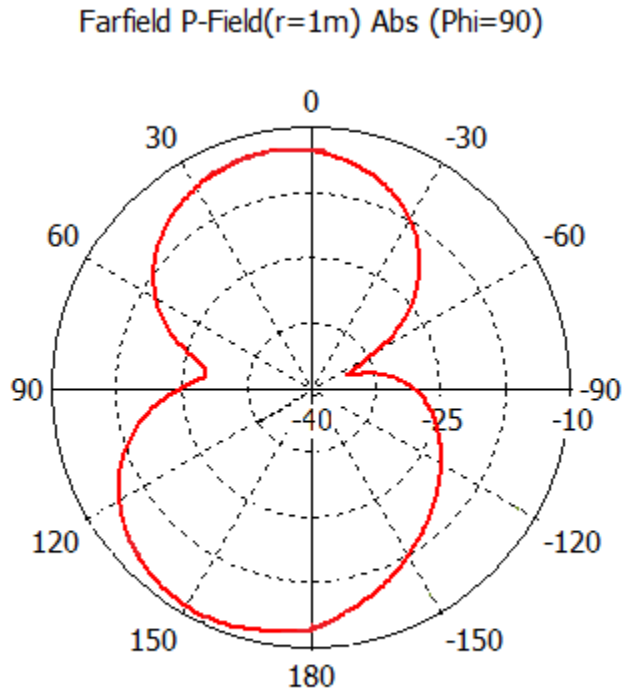

(c) yz-plane (f=5.75 GHz)

Figure 4.21:(a),(b),(c) radiation pattern of the third designed antenna

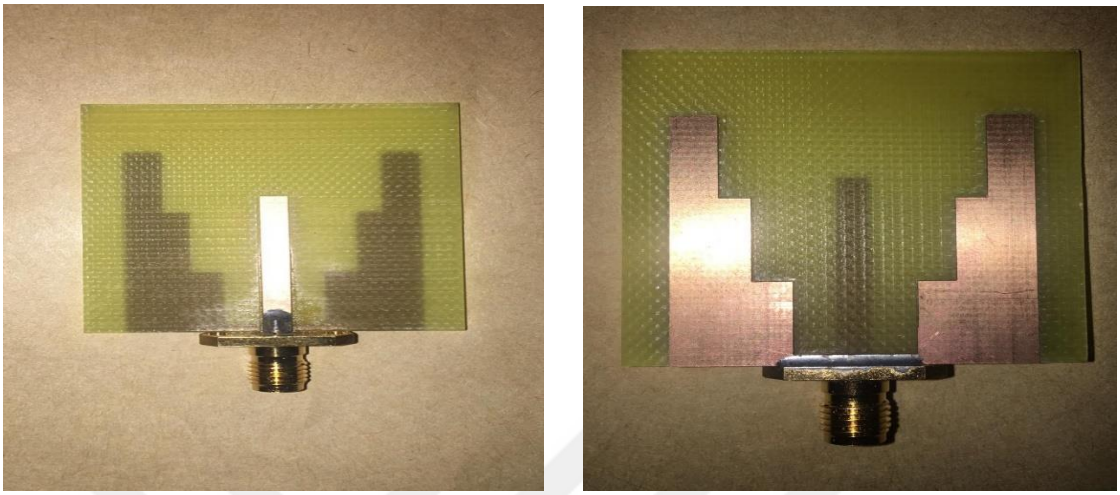

(a) (b)

Figure 4.22: explains the (a) top-view, (b) bottom-view of fabricated antenna prototype.

Figure 4.23 explains the simulated and measured S_{11} responses of printed slot antenna. Both are in good agreement. Trivial variations of simulated and measured responses are due to fabrication tolerance as well as simulation adjusted accuracy.

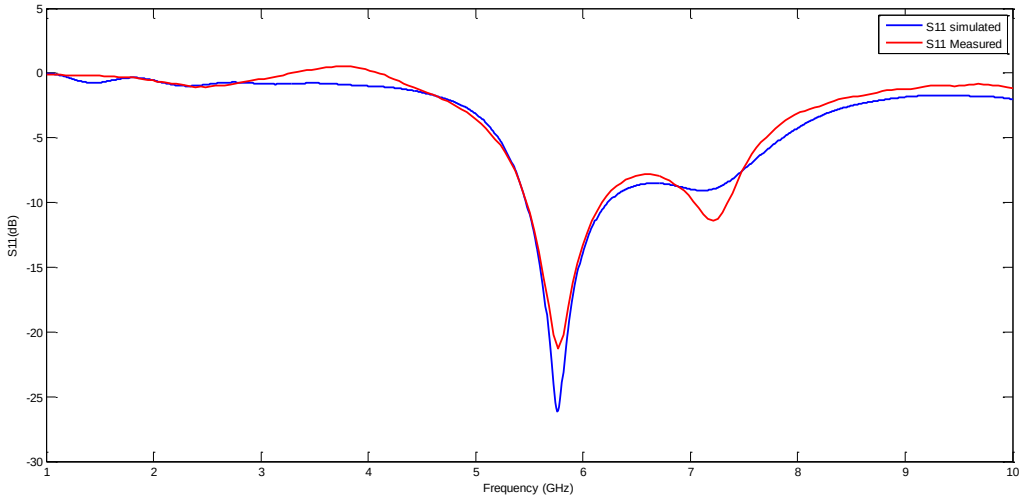

Figure 4.23: The simulated and measured S_{11} responses of printed slot antenna.

5. CONCLUSIONS AND RECOMMENDATIONS FOR FUTURE WORK

5.1 CONCLUSIONS

The aim of this thesis is to present design antennas with single, dual and multi band resonance in order to cover the recently available communication services. By using FR4 substrate material, two microstrip antennas based on quasi fractal geometries are presented. They have clearly multi band response for modern wireless applications. This antenna has modeled using AWR simulator based on quasi-fractal topology. The shaped antenna has compacted size and acceptable electrical specifications that are suitable for numerous fixed and handheld wireless systems.

The third designed device is printed slot antenna and does not stand for microstrip antenna just the feed is microstrip since the designed stair-step topology has been printed in the ground plane of FR4 substrate. Based on the parametric study of third antenna, its response has only single and dual potential bands. Here in this study, single band response at strategic frequency of 5.75 GHz has been adopted with fabrication and measurements.

5.2 RECOMMENDATIONS FOR FUTURE WORK

Based on the work reported in this thesis, several points have been noticed to be tried to satisfy the goal as a future work. These points can be summarized as follows:

1. Attempting other types of fractal geometries which might add additional features to the resulting printed slot antenna structures, such size miniaturization and gain enhancement together with the required dual and wide-band response.
2. Adding new requirements to the resulting dual-band antenna design; such as it has to successfully pass the tests of its employment in the ever spread technology of the MIMO (multi input multi output) applications.
3. Fabricating the 1^{st} and 2^{nd} antenna as future work after receiving the adequate funds.

REFERENCES

[1] Bayat, Oguz, Webert Montlouis, Bahram Shafai, Osman N. Ucan, and Onur Osman. "Channel estimation and tracking of wireless communication." In MILCOM 2005-2005 IEEE Military Communications Conference, pp. 214-217. IEEE, 2005.

[2] Rasheda, Hamid Mohammed Qasem, and H. Mohammed. "Ultra Wideband Antenna for Microwave Imaging Using Modified Fractal Structure." PhD diss., Universiti Tun Hussein Onn Malaysia, 2017.

[3] Fractal Antenna Construction, Available [online]: http://www.scienceprog.com/fractal-antenna-constructions/

[4] Fractal, Available [online] : http://mathworld.wolfram.com/Fractal.html

[5] G. Kumar, and K. P. Ray, "Broadband Microstrip Antennas", Artech House, Inc., Boston, London, 2003.

[6] R. Bancroft, "Microstrip and Printed Antenna Design", 2nd Ed., SciTech Publishing, Inc., Raleigh, NC, 2009.

[7] C. A. Balanis, "Antenna Theory: Analysis and Design", 3rd Ed., John Wiley & Sons, Inc., Hoboken, New Jersey, 2005.

[8] Z. N. Chen, and M. Y. W. Chia, "Broadband Planar Antennas Design and Applications", John Wiley & sons, Ltd, England, 2006.

[9] R. Garg, P. Bhartia, I. Bahl, and A. Ittipiboon, "Microstrip Antenna Design Handbook", Artech House, Inc., Boston, London, 2001.

[10] Karamzadeh, S., V. Rafii, M. Kartal, O. N. Ucan, and Bal S. Virdee. "Circularly polarised array antenna with cascade feed network for broadband application in C-band." Electronics Letters 50, no. 17, 2014.

[11] B. B. Mandelbrot, "The Fractal Geometry of Nature", W. H. Freeman, San Francisco, CA, 1982.

[12] Bellido, Edson P., Gabriel D. Bernasconi, David Rossouw, Jérémy Butet, Olivier JF Martin, and Gianluigi A. Botton. "Self-Similarity of Plasmon Edge Modes on Koch Fractal Antennas." *ACS nano* 11, no. 11 (2017): 11240-11249.

[13] Jawad K. Ali, M. T. Yassen, M. R. Hussan, and A. J. Salim, " A Printed Fractal Based Slot Antenna for Multi-band Wireless Communication Applications", Progress In Electromagnetics Research, PIER Proceedings, Moscow, Russia, August 19-23, 2012.

[14] D. Li, F. -S. Zhang, Z. -N. Zhao, L. -T. Ma, and X. -N. Li, " A CPW-fed Wideband Koch Snowflake Fractal Monopole for WLAN/WiMAX Applications", Progress In Electromagnetics Research C, PIER, Vol. 28, pp. 143-153, 2012.

M. R. Haji-Hashemi, H. Mir-Mohammad Sadeghi, and V. M. Moghtadai, " Space-filling Patch Antennas with CPW Feed ", Progress In Electromagnetics Research Symposium, Cambridge, USA, March 26-29, 2006.

[16] P. S. Addison, "Fractals and Chaos", Institute of Physics Publishing, IOP, Ltd, London, 1997.

[17] Jawad K. Ali, "Microstrip-fed Printed Slot Antennas Based on Hilbert-Type Space-Filling Curves for Wireless Communication Systems ", International Review on Modelling and Simulations, I.RE.MO.S, Vol. 3, No. 4, August, 2010.

[18] Pia, Giorgio. "Fluid flow in complex porous media: Experimental data and IFU model predictions for water vapour permeability." *Journal of Natural Gas Science and Engineering*35 (2016): 283-290.

[19] Llorens-Quintana, Clara, and D. Robert Iskander. "Assessment of tear film using videokeratoscopy based on fractal dimension." *Optometry and Vision Science* 95, no. 1 (2018): 32-42.

[20] Abbena, Elsa, Simon Salamon, and Alfred Gray. *Modern differential geometry of curves and surfaces with Mathematica*. Chapman and Hall/CRC, 2017.

[21] Nash, John C. *Compact numerical methods for computers: linear algebra and function minimisation*. Routledge, 2018.

[22] Bryson, Arthur Earl. *Applied optimal control: optimization, estimation and control*. Routledge, 2018.

[23] Natanson, Isidor Pavlovich. *Theory of functions of a real variable*. Courier Dover Publications, 2016.

[24] Boiangiu, C., Adrian G. Morosan, and Marian Stan. "A fractal world: building visually-rich and fully-realistic natural environments." *Int. J. Math. Comput. Simul* 10 (2016): 100-111.

[25] Bellido, Edson P., Gabriel D. Bernasconi, David Rossouw, Jérémy Butet, Olivier JF Martin, and Gianluigi A. Botton. "Self-Similarity of Plasmon Edge Modes on Koch Fractal Antennas." *ACS nano* 11, no. 11 (2017): 11240-11249.

[26] Fang, Sizhen, Dylan A. King, Eun Bi Lee, and Robert S. Strichartz. "Spectral decimation for families of self-Similar symmetric Laplacians on the Sierpinski gasket." *arXiv preprint arXiv:1709.02031* (2017).

[27] Bannink, Tom, and Harry Buhrman. "Quantum Pascal's Triangle and Sierpinski's carpet." *arXiv preprint arXiv:1708.07429* (2017).

[28] Cao, Thanh Nghia, and Wojciech J. Krzysztofik. "Hybrid Minkowski fractal island antenna operating in two bands of GPS satellite system." In *2016 IEEE International Symposium on Antennas and Propagation (APSURSI)*, pp. 211-212. IEEE, 2016.

[29] Chowdary, P. Satish Rama, A. Mallikarjuna Prasad, P. Mallikarjuna Rao, and Jaume Anguera. "Design and performance study of Sierpinski fractal based patch antennas for multiband and miniaturization characteristics." *Wireless Personal Communications* 83, no. 3 (2015): 1713-1730.

[30] Moreno, Jaime, Oswaldo Morales, Ricardo Tejeida, Juan Posadas, Hugo Quintana, and Grigori Sidorov. "Distributed Learning Fractal Algorithm for Optimizing a Centralized Control Topology of Wireless Sensor Network Based on the Hilbert Curve L-System." *Sensors* 19, no. 6 (2019): 1442.

[31] Ali Rashid Al-Salihi, Osman Nuri Ucan, Yaqeen Sabah Mezaal, Oguz Bayat, Hussein Ali Hussein. “Design and Simulation of Quasi-Fractal Microstrip Antennas for Wireless Communication”, International Journal of Electronics, Submitted (manuscript ID is TETN-2019-0628).

[32] Ashikhmin, Aleksandr V., Alexander V. Negrobov, Yuriy G. Pasternak, Pavel V. Pershin, and Sergey M. Fedorov. "Quasi-fractal antenna system based on asymmetric TEM-horns nested into each other." *Microwave and Optical Technology Letters* 60, no. 2 (2018): 322-324.

[33] Khan, Sebastian, Sascha Husa, Mark Hannam, Frank Ohme, Michael Pürrer, Xisco Jiménez Forteza, and Alejandro Bohé. "Frequency-domain gravitational waves from nonprecessing

black-hole binaries. II. A phenomenological model for the advanced detector era." *Physical Review D* 93, no. 4 (2016): 044007.

[34] Jawad K. Ali and Seevan F. Abdulkareem, "A Circle-based Fractal Slot Antenna for Dual-band Wireless Applications", To Be Published in the Proceedings of the IEEE Mediterranean Microwave Conference, MMS 2013, Saida, Lebanon, 3-5 September. 2013.

[35] N. Poprzen, and M. Gacanovic, "Fractal Antennas: Design, Characteristics and Application ", Regular Paper, 2000.